NTNU

Norwegian University of
Science and Technology

Incoporating Ammonia Synthesis for an Offshore Gas-to-Liquid Process

Mathias Kristoffer Lundgren

Chemical Engineering and Biotechnology
Submission date: June 2016
Supervisor: Magne Hillestad, IKP

Norwegian University of Science and Technology
Department of Chemical Engineering

Abstract

The world energy demand is increasing, and so is the demand for fertilizer to sustain an exponential population growth. Currently, with low oil prices, associated natural gas is flared off or re-injected into oil reservoirs for enhanced oil recovery (EOR). A gas-to-liquid process (GTL) for offshore applications aboard a floating production, storage, and offloading vessel (FPSO) incorporating Fischer-Tropsch Synthesis (FTS) seeks to reform natural gas into more valuable liquid products. As the composition of natural gas feeds varies greatly depending on location and other factors, a surplus of hydrogen production is maintained in order to have a steady production of the desired FTS products. An alternative use for this surplus hydrogen is in ammonia synthesis, which in a relatively simple process design using readily available streams in the GTL process, can produce considerable amounts of ammonia.

A complimentary design to an existing GTL process designed for offshore applications which seeks to incorporate ammonia synthesis is proposed. Two possible designs are tentatively suggested and evaluated, each design utilising different streams in the GTL process with a high nitrogen content, in addition to the surplus hydrogen stream in the GTL process. The process design features a synthesis loop, as well as removal of compounds containing oxygen, such as CO_2 and water, as these compounds are poisonous to the ammonia synthesis catalyst. The ammonia synthesis reactor is simulated as three separate beds, with a refrigeration loop to cool the stream exiting the reactor to sub-zero temperatures in order for ammonia to condense and be separated from the synthesis loop. Uncondensed ammonia and unreacted hydrogen and nitrogen gas is recycled and reintroduced to the reactor.

Two separate process designs were simulated in Aspen HYSYS V8.6, each with a different source of nitrogen. The basis for the nitrogen sources for the ammonia synthesis process are the streams pertaining to the GTL process proposed by Hillestad *et.al.* [17]. Two different kinetic models were also evaluated. Heat integration is performed in Aspen Energy Analyzer V8.6, and a heat exchanger network (HEN) is proposed.

The best process design features the N_2-rich stream from the membrane in the air enrichment unit in the GTL process, as this offers a simpler process

design compared to utilising the tailgas from the GTL process. The system is optimised using the Temkin-Pyzhev kinetic model for the ammonia synthesis reactor. The power-optimal operating pressure is found to be approximately 235 bar, while the optimal operating temperature is found to be approximately 415 °C depending on the reaction bed.

After heat integration, the process requires no external heat source, and the system power demand is sufficiently low to be met by the gas turbine in the GTL process. The process converts 1889 kgmol/h of unprocessed hydrogen/CO_2 stream from the hydrogen selective membrane in the GTL process, and 613 kgmol/h of nitrogen/oxygen stream from the air enrichment unit to produce 1167 kgmol/h, or 19.9 tons/h, of ammonia. The total investment cost of the proposed design is estimated to 87.6 million US$.

Sammendrag

Verdens energibehov øker, og det gjør også behovet for kunstgjødsel for å imøtekomme en eksponensiell populasjonsvekst. I skrivende stund er spottprisen for olje så lav at assosiert naturgass enten fakles eller reinjiseres i oljereservoarer for å øke produksjonen som følge av utfordringer med å transportere gassen til land for å prosessere den. En gass-til-væske-prosess (GTL) som benytter seg av Fischer-Tropsch-syntese (FTS) reformerer naturgassen til mer verdifulle fraksjoner. Ettersom sammensetningen av naturgassen varierer, blir hydrogen produsert i overskudd for å vedlikeholde produksjonen av den ønskede FTS-fraksjonene. Et alternativt bruksområde for dette overskuddet er ammoniakkproduksjon som kan benytte seg av strømmer allerede tilstede i GTL prosessen og et relativt enkel prosessdesign, til å produsere store mengder ammoniakk.

Et komplimentert prosessdesign til en eksisterende GTL prosess som er designet for offshore produksjon av ammoniakk er foreslått. To forskjellige design er foreslått, hvor hver av dem tar i bruk forskjellige nitrogenkilder i et eksisterende prosessdesign for en GTL-prosess. Det foreslåtte prosessdesignet benytter seg også av overskuddet med hydrogen. Den foreslåtte prosessen innebærer fjerning av oksygenholdige stoffer som CO_2 og vann, ettersom disse stoffene er giftige for katalysatoren benyttet i ammoniakksyntese. Ammoniakk blir produsert i en synteseloop, som er simulert som en reaksjon som foregår over tre trinn i reaktoren med kjling mellom hvert trinn. En kjøleprosess som kjøler ned ammoniakken slik at den kan kondensere og separeres ut fra synteseloopen ble også simulert. Ureagert nitrogen og hydrogen, samt ukondensert ammoniakk blir resirkulert tilbake til først trinn i reaktoren.

To forskjellige prosessdesign ble simulert i Aspen HYSYS V8.6 hvor hver av dem tar i bruk forskjellige nitrogenkilder i det eksisterende prosessdesign GTL prosess foreslått av Hillestad *et.al.* [17]. To forskjellige kinetikkmodeller ble undersøkt som modeller for ammoniakksyntese. Varmeintegrering av prosessen ble gjennomført i Aspen Energy Analyzer V.8.6 og er varmevekslernettverk ble foreslått.

Det mest vellykkede prosessdesignet tok i bruk den nitrogenrike strømmen fra luftanrikningsenheten i GTL prosessen, ettersom denne strømmen krever et min-

dre intrikat prosessdesign uten å tape for mye hydrogen i bearbeidingen av nitrogenstrømmen sammenliknet med å benytte seg av avfallsstrømmen fra gassturbinen. Systemet ble optimalisert ved bruk av Temkin-Pyzhevs kinetikkmodell for ammoniakkproduksjon. The optimale trykket i reaktoren med hensyn på kraftforbruk ble funnet å være på ca. 235 bar. Den gjennomsnittlige optimale temperaturen i reaktoren ble funnet å være ca. 415 °C men varierer med forskjellige trinn i reaktoren.

Etter at prosessen ble varmeintegrert har den ikke behov for ekstern oppvarming og kraftforbruket i hele prosessen var lavt nok til å dekkes av gassturbinen i GTL prosessen. Prosessen omdanner 1 889 kmol/t med uprosessert hydrogenstrøm som inneholder hydrogen og karbondioksid fra en hydrogenselektiv membran, samt 613 kmol/t med uprosessert nitrogenstrøm som inneholder nitrogen og oksygen, og omdanner disse strømmene til 1167 kmol/t (19.9 tonn/t) med ammoniakk. Den totale investeringskostnaden er estimert til 87,6 millioner US$.

Preface

This report is the product of my thesis work for my M.Sc. degree i chemical engineering at the Norwegian University of Science and Technology (NTNU) spring semester, 2016. The work was done at the Department of Chemical Enigneering as part of the research group of Environmental Engineering and Reactor Technology.

The thesis work encompassed process design, simulation, optimisation and evaluation of an ammonia synthesis process which was to be integrated into an existing offshore gas-to-liquid process design using Aspen HYSYS and Aspen Energy Analyzer.

I wish to thank my supervisor, Magne Hillestad for his diligent guidance and concrete advise whenever I encountered problems in my work. I also wish to thank my co-supervisor, Mohammad Ostadi for his technical support when I encountered issues with the simulation.

I will also like to thank my fellow chemical engineering students for wonderful years at NTNU.

"I hereby declare that this is an independent work according to the exam regulations of the Norwegian University of Science and Technology (NTNU)"

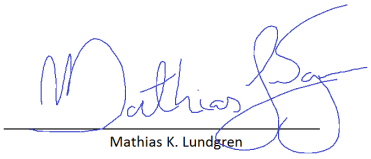

Mathias K. Lundgren

Contents

List of Tables

List of Figures

Abbreviations

ACM	Aspen Custom Modeller
ASU	Air Separation Unit
ATR	Autothermal Reformer
CEPCI	Chemical Engineering Plant Cost Index
EOR	Enhanced Oil Recovery
FPSO	Floating Production, Storage and Offloading
FTS	Fischer-Tropsch Synthesis
GHSV	Gas Hourly Space Velocity
GTL	Gas-To-Liquid
HEN	Heat Exchanger Network
HER	Heat Exchange Reformer
HI	Heat Integration
HP	High Pressure
ISBL	Inside Battery Limits
LP	Low Pressure
MMBTu	Million British Thermal Unit
MP	Medium Pressure
OSBL	Outside Battery Limits
PCE	Total Equipment Cost
PPC	Installed Equipment Cost
RDS	Rate Determining Step
WGS	Water-Gas Shift

Nomenclature

Chapter 2

*	Free catalytic site
C_3	Hydrocarbon chain og 3 carbon atoms
C_5	Hydrocarbon chain og 5 carbon atoms
C_{5+}	Hydrocarbon chain og 5 carbon atoms or longer
C_9	Hydrocarbon chain og 9 carbon atoms
C_{11}	Hydrocarbon chain og 11 carbon atoms
C_{25}	Hydrocarbon chain og 25 carbon atoms
$H_2{}^*$	H_2 adsorbed on catalytic site
n	Arbitrary stoichiometric coefficient
N_2^*	N_2 adsorbed on catalytic site
NH^*	NH adsorbed on catalytic site
$NH_2{}^*$	NH_2 adsorbed on catalytic site
$NH_3{}^*$	NH_3 adsorbed in vatalytic site
w_i	Weight fraction of component i
α	Chain growth probability factor
ΔH	Heat of reaction
ΔH_{298}	Heat of reaction at 298K
ΔT_{min}	Minimal temperature difference between a hot and a cold stream

Chapter 3

A	Pre-exponential factor
E_a	Activation energy
k_{-1}	Backwards reaction rate constant
k_1	Forwards reaction rate constant
p_{H_2}	Hydrogen partial pressure
p_{N_2}	Nitrogen partial pressure
p_{NH_3}	Ammonia partial pressure
r_{-1}	Backwards reaction rate
r_1	Forward reaction rate
r_{NH_3}	Ammonia foration rate
R	Universal ideal gas constant
T	Temperature
ϕ_{H_2}	Fugacity of hydrogen gas
ϕ_{N_2}	Fugacity of nitrogen gas
ϕ_{NH_3}	Fugacity of ammonia

Chapter 4

$\dot{N}_{Fresh}$	Molar flowrate of fresh stream entering the synthesis loop
$\dot{N}_{Recycled}$	Molar flowrate of recycled components in the synthesis loop
R	Recycle ratio
T_{in}	Temperature at inlet
T_{out}	Temperature at outlet
ΔT	Temperature change

Appendix C

$\dot{m}_{in}$	Mass flowrate in
$\dot{m}_{out}$	Mass flowrate out
$d\%$	Discrepancy percentage
Q_{in}	Heat entering a steady state system
Q_{out}	Heat leaving a steady state system
$\dot{Q}_{in}$	Heat flowrate into a system
$\dot{Q}_{out}$	Heat flowrate out of a system
W_{in}	Work done on a system
W_{out}	Work done by a system

Appendix E

T_{in}	Temperature at inlet
T_{out}	Temperature at outlet

Appendix F

A_h	Eliptical head surface area
A_s	Surface area of a cylinder/vessel
D_{outer}	Outer diameter of the vessel
D_v	Vessel inner diameter
E	Welding efficiency factor
GHSV	Gas hourly space velocity
H	Vessel inner height
H_h	Outer hight of the eliptical head
H_{outer}	Outer hight of the vessel
m	Mass
P	Design pressure
S	Allowable stress
S.F	Straight flange
t	Time
t_w	Vessel shell thickness
u_s	Settling velocity
$\dot{V}_g$	Volumetric gas flow rate
V_{shell}	Vessel shell volume
V_{tot}	A vessels outer volume
ρ_g	Gas density
ρ_l	Liquid density
ρ_m	Vessel material density

Appendix G

a	Eqipment purchase cost calculation factor
b	Eqipment purchase cost calculation factor
C_e	Equipment purchase cost
f_1	Equipment erection factor
f_2	Piping factor
f_3	Instrumentation and controll factor
f_4	Electrical factor
f_5	Material factor
f_6	Utilities factor
f_7	Lagging and pain factor
f_8	Design and engineering factor
n	Eqipment purchase cost calculation factor
S	Eqipment purchase cost calculation factor

Chapter 1

Introduction

There is no question that gas technology has developed over the last decade. Until recently, high oil prices have forced the market to shift towards the production and processing of natural gas simply to meet a market unsaturated with the need for hydrocarbon fuels. In the wake of this change in energy policy, there has been a reinvigoration of Fischer-Tropsch synthesis (FTS), a technology employed by the Germans during World War II as a means of fuel production. However, with the recent drop in oil prices, the profitability margin of Fischer-Tropsch products has all but disappeared.

Many attribute the unprecedented world population growth seen in the last century to another German invention, namely the Haber-Bosch process for ammonia production [6]. Without this process, the amount of land needed for cultivation to feed the currently 7 billion people on this planet would be 4 times what it is today compared to a century ago [21], as ammonia serves as the main feedstock for the world's fertilizer production. Ammonia has a market nearly impossible to saturate, as there are currently no government stockpiles of ammonia [20]. Historically there has been a correlation between market price of natural gas and ammonia, as the former serves as a feedstock for the production of the latter[18]. However, over the last few years, there has been a decoupling of this correlation as ammonia prices have increased while natural gas prices have decreased, as shown in Figure 1.1 [18].

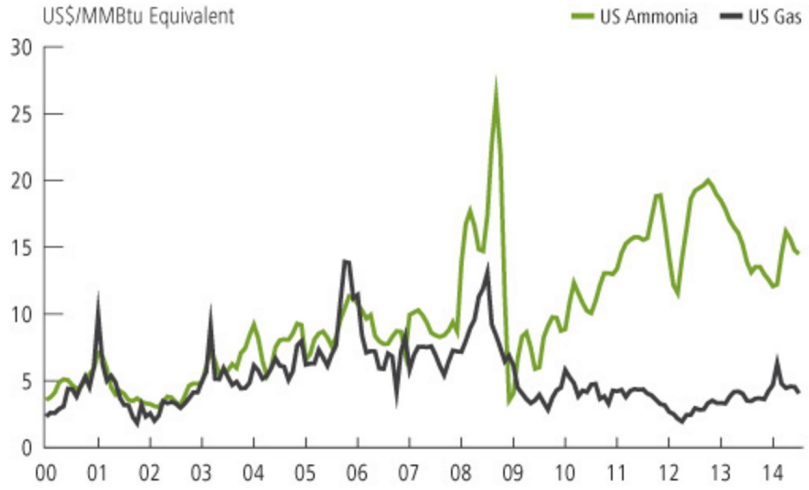

Figure 1.1: The historical correlation between ammonia and natural gas prices in the US.

This in turn increases the profitability margin for ammonia production.

As the spot price for crude oil, and in turn the market price for processed fuels, is notoriously difficult to predict, a complimentary scheme to natural gas reforming to produce ammonia would alleviate some of the economic risk if a process could prioritise one product over the other as market prices change. As the both Fischer-Tropsch synthesis and ammonia synthesis both require much of the same processing, such as air enrichment, pre-treating of natural gas, and the production of hydrogen, synergy between the two processes could prove quite profitable if implemented in a process design which incorporates both processes.

A process which could produce both FTS products and ammonia would offer flexibility as the price for each product fluctuates, which in turn would provide more financial security. In addition, the combined process would likely require less power consumption, as they both share energy intensive processes such as an air enrichment unit and pre-treating of natural gas. Combined they could potentially reduce the energy requirement compared to if they are run as independent processes.

1.1 Objective

The thesis objectives, which were outlined at the beginning of the project with thesis supervisor Professor Magne Hillestad, were to examine the possibility of incorporating ammonia synthesis into an existing offshore GTL process, specifically for a FPSO. The process design had at its disposal two sources of nitrogen for ammonia synthesis, both seemingly viable options. The process was to be

implemented with a kinetic model to accurately simulate the system. Full optimisation with respect to operating conditions of the ammonia synthesis process was to be performed, as well as heat integration of the process, and sizing and cost estimation of the process equipment.

1.2 Acknowledgements of Contribution

The Process design and Aspen HYSYS simulation for the GTL process were developed by Professor Hillestad, Kristin Dalane and Mohammed Ostadi [17].

My own main contributions are (but not limited to):

1. Developing the process design for an ammonia synthesis process with two different sources of nitrogen, each coming from the GTL process.
2. Implementing two different kinetic models for ammonia synthesis.
3. Evaluation and optimisation of the proposed system designs and kinetic models.
4. Heat integration of the process by using Aspen Energy Analyzer V8.6.
5. Sizing and cost estimation for the optimised system.

1.3 Thesis Structure

Chapter 2 will be devoted to the explanation of the process outline of the existing GTL process, and how the ammonia synthesis unit can be incorporated. It will also deal with the underlying theory and the mechanisms involved in ammonia synthesis, as well as the concept of heat integration and process design pertaining to a FPSO.

Chapter 3 will explain the basis for the simulation performed in Aspen HYSYS. It will define the input streams and the different configurations and kinetics which are to be examined. It will also outline how the heat integration was performed and define the utility streams.

Chapter 4 will present and discuss the results which were obtained through the simulation of the different options pertaining to the ammonia synthesis process design. It will evaluate two different kinetic models. Optimisation of the implemented kinetic model and the system design will be thoroughly performed before a heat exchanger network is suggested for the process. The finalised, heat integrated process design will have its equipment properly sized and cost estimated.

Chapter 5 will present the findings from the optimised process and present topics for further work.

Chapter 2

Ammonia Synthesis Steps

2.1 Process Outline

The proposed process will use steam reforming of natural gas to produce C_{5+} alkanes through Fischer-Tropsch Synthesis (FTS) in a gas-to-liquid process (GTL), and using the surplus hydrogen from the FTS and one of two possible nitrogen sources to produce ammonia. The aim is for the process to be viable for offshore applications on board a floating production- storage- and offloading vessel (FPSO). A block diagram of the process is given in Figure 2.1.

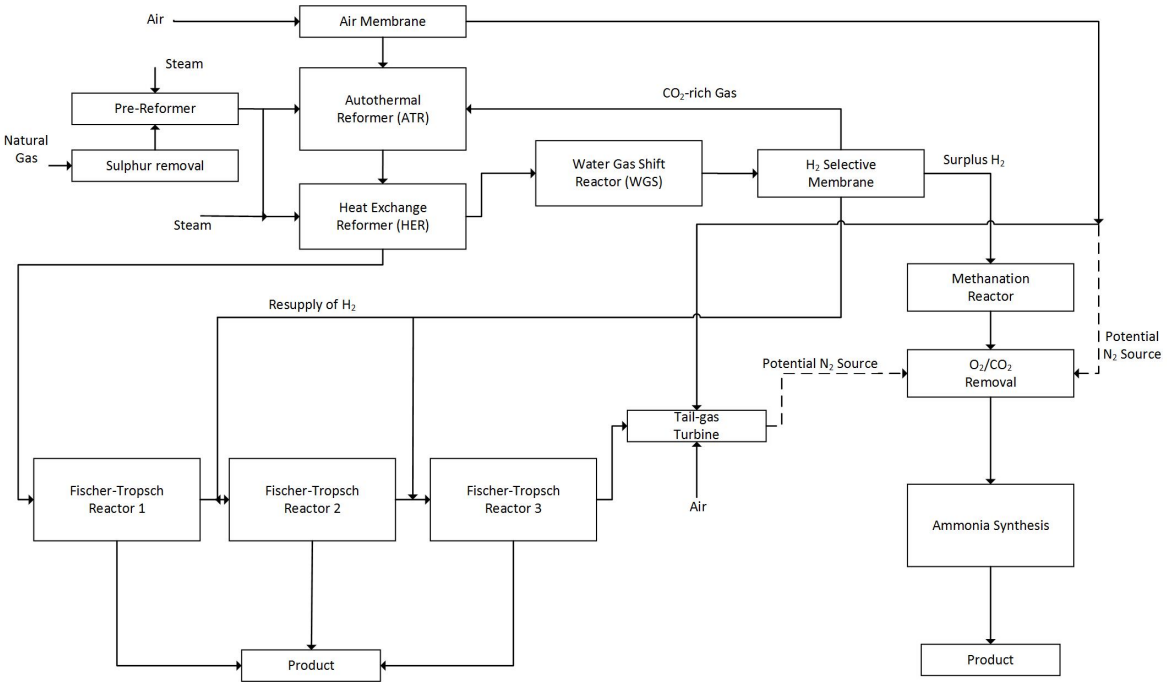

Figure 2.1: A block diagram for the proposed process

2.1.1 The Existing GTL Process

The GTL process was developed by Hillestad *et. al.*[17]. It employs the use of micro-channel reactors for FTS modelled by Ostadi [16] and the Heat exchange Reformer (HER) Falkenberg [5] in Aspen Custom Modeller (ACM).

The process feedstock is a 6 000 kmol/h stream of natural gas, which is composed of 95% methane, 2% ethane, 3% C_3 - C_5 alkanes . An air enrichment unit supplies the auto thermal reformer (ATR) with a high oxygen content stream, where it is mixed with steam and 90% of the natural gas feed.

A heat exchange reformer (HER) is supplied the stream from the ATR and the remaining with 10% of the natural gas feed, and additional steam. The stream then splits, where one stream is sent to the first FTS reactor, while the other is sent to a high temperature water gas shift (WGS) reactor. The WGS reactor will produce additional hydrogen, which will pass through a hydrogen selective membrane to remove the bulk of the CO_2 present in the stream. Some of the hydrogen is then injected into FTS reactor number 2 and 3 according to the H_2/CO ratio described in Section 2.1.2, while the surplus is sent to storage.

After each FTS reactor, the heavier hydrocarbons are separated out and combined with the condensate of the other FTS reactors to make up the product

stream. After the third FTS reactor, the stream is referred to as the tailgas, which contains unconverted syngas as well as small amounts of hydrocarbons. The tailgas is resupplied with compressed air, and the nitrogen rich stream from the air enrichment unit, and combusted in a gas turbine which will supply the process with electrical power.

2.1.2 Fischer-Tropsch Synthesis

Fischer-Tropsch synthesis is a process in which syngas, a mixture of carbon monoxide and hydrogen gas, is converted into hydrocarbons of a desired carbon chain length according to Equations 2.1, paraffin formation, and 2.2, olefin formation[3].

$$\mathrm{nCO} + (2\,\mathrm{n} + 1)\,\mathrm{H_2} \longrightarrow \mathrm{C_nH_{2n+2}} + \mathrm{nH_2O} \tag{2.1}$$

$$\mathrm{nCO} + (2\,\mathrm{n})\mathrm{H_2} \longrightarrow \mathrm{C_nH_{2n}} + \mathrm{nH_2O} \tag{2.2}$$

The FTS products have a wide distribution of carbon chain lengths from methane up to heavy waxes. The distribution of hydrocarbon chain length is a statistical model, named the Anderson-Schults-Flory distribution [3], given in Equation 2.3.

$$w_i = i(1-\alpha)^2\alpha^{i-1} \tag{2.3}$$

where w_i is the weight fraction and i is the number of carbon atoms in the chain, and α is the chain growth probability factor.

The chain length is influenced by a number of factors, such as operating temperature, catalyst type, and the ratio of H_2 to CO. A high H_2/CO ratio will increase selectivity towards short hydrocarbon chains. It is therefore important to regulate this ratio in order to produce the desired carbon chain length. For high valuable products, such as gasoline (C_5 - C_{11}) and diesel (C_9 - C_{25}), a low H_2/CO ratio is favourable. In the design put forward by Hillestad *et. al.*[17], a H_2/CO of 2 is used. As hydrogen is consumed in the FTS reactors, additional hydrogen is supplied to the consecutive reactors to maintain the H_2/CO ratio. However, there is a surplus of produced hydrogen gas, as three parts H_2 and one part CO is produced for every 1 part methane, according to Equation 2.4 which is know as high temperature steam reforming of methane.

$$\mathrm{CH_4(g)} + \mathrm{H_2O(g)} \rightleftharpoons \mathrm{CO(g)} + 3\,\mathrm{H_2(g)} \qquad \Delta H_{298\mathrm{K}} = 206.3\,\mathrm{kJ/mol} \tag{2.4}$$

In the GTL process described in Figure 2.1, some of the syngas is used for production of additional hydrogen in the WGS reactor according to Equation 2.5, known as the water-gas shift reaction.

$$CO(g) + H_2O(g) \rightleftharpoons CO_2(g) + H_2(g) \qquad \Delta H_{298K} = -41.16\,kJ/mol \quad (2.5)$$

While maintaining a H_2/CO ratio of 2, there is a substantial surplus stream of hydrogen which can be used for product upgrading when the FPSO offloads its products onshore, or, as this thesis with examine, the surplus hydrogen can be used for ammonia synthesis.

2.2 Ammonia Production

Ammonia synthesis is one of the most thoroughly examined areas in industrial chemistry. This is due to its uses in the manufacturing of nitrogen-based fertilizers such as ammonium nitrate and urea. The annual global production of ammonia was estimated at 146 million metric tons in 2015 [15], with approximately 88% going towards fertilizer production[15]. The production of ammonia requires two key components, a hydrogen source and a nitrogen source.

2.2.1 Hydrogen Production

In conventional industrial applications, the hydrogen is supplied by steam-reforming natural gas, given in Equation 2.4. The resulting formation of carbon monoxide is further reacted with water to yield even more hydrogen in the water-gas shift reaction, shown in Equation 2.5.

Hydrogen can alternatively be produced in a semi-batch process by using high pressure steam over an iron catalyst to yield iron(II) oxide and hydrogen gas, or through electrolysis, but the net energy requirement for these two processes are far higher than the aforementioned mechanisms.

2.2.2 Nitrogen Production

The nitrogen required for ammonia synthesis is conventionally produced by using an air separation unit (ASU)[13]. Though this process primarily aims to separate oxygen from other inert atmospheric components such as nitrogen, argon and carbon dioxide, a relatively pure nitrogen stream is nevertheless a bi-product in this process. This process is further sub-categorised into cryogenic- and non-cryogenic ASU. Cryogenic separation requires a more complex operation than non-cryogenic separation in certain cases, but delivers separation products with higher purity than non-cryogenic separation is able to produce. In cases where only air enrichment is required, membrane technologies can be employed. These membranes require much less energy to separate the atmospheric components, but do so at the expense of purity. Polymeric (typically yielding around 25-50% oxygen)[12] and ceramic membranes (such as oxygen

transport and ion transport membranes, which can achieve up to 90% pure oxygen[12]) can be used, but they have individual temperature requirements. Polymeric membranes only require ambient/warm temperatures, while ceramic membranes require temperatures in the 800-900 °C range[12].

In the case of the air separation unit for the proposed system design, a ceramic membrane is used to provide air separation to yield a 90% oxygen separation before entering the ATR. The key reasons for not using a cryogenic ASU to yield pure oxygen for use in the ATR are threefold. One reason is that having a pure oxygen stream in the vicinity of volatile hydrocarbon streams constitutes a major fire and explosion hazard. Secondly, having a pure oxygen stream really is not necessary in the proposed design and using a cryogenic ASU would impose greater energy constrains on the system than required. Finally, conventional ASUs require large rectification columns which are not possible to safely operate on a FPSO even if the spatial constrains were not an issue, which they clearly are.

2.2.3 The Haber-Bosch Process

Ammonia production takes place in a synthesis loop in a process known as the Haber-Bosch process where hydrogen gas reacts with nitrogen gas, conventionally over an iron catalyst, to form ammonia according to Equation 2.6 [13].

$$\mathrm{N_2(g)} + 3\,\mathrm{H_2(g)} \overset{Fe}{\rightleftharpoons} 2\,\mathrm{NH_3(g)} \qquad \Delta H = -92.4\,\mathrm{kJ/mol} \tag{2.6}$$

The catalytic reaction is a non-elementary reaction, and follows the catalytic steps outlined in Equations 2.7 to 2.14[6][9]:

$$\mathrm{N_2} + {}^* \longrightarrow {N_2}^* \tag{2.7}$$
$${N_2}^* \longrightarrow 2\,\mathrm{N}^* \tag{2.8}$$
$$\mathrm{H_2} + {}^* \longrightarrow {H_2}^* \tag{2.9}$$
$${H_2}^* \longrightarrow 2\,\mathrm{H}^* \tag{2.10}$$
$$\mathrm{N}^* + \mathrm{H}^* \longrightarrow \mathrm{NH}^* \tag{2.11}$$
$$\mathrm{NH}^* + \mathrm{H}^* \longrightarrow {NH_2}^* + {}^* \tag{2.12}$$
$$\mathrm{NH}^* + \mathrm{H}^* \longrightarrow {NH_3}^* + {}^* \tag{2.13}$$
$${NH_3}^* \longrightarrow \mathrm{NH_3} + {}^* \tag{2.14}$$

The overall reaction rate is governed by the rate determining step (RDS), which from experimental data is likely to be the second step, Equation 2.8. This step requires a great deal of heat as the nitrogen-nitrogen bond has to be broken,

and this triple covalent bond is one of the strongest chemical bonds in nature [13]. As a result, high temperature is required in the Haber-Bosch process to initiate, which are not favourable conditions for the overall reaction. As stated in Equation 2.6, the reaction is exothermic, which means a low temperature is required for maximum conversion. Hence there is a trade-off with respect to temperature in an ammonia synthesis reactor. If the temperature is too high, the reaction proceeds slowly as ammonia decompose back into N_2 and H_2 at high temperatures, but if the temperature is too low, the activation energy required for the RDS will be too high for the reaction to proceed. This is the main reason why ammonia synthesis takes place in a loop where unreacted N_2 and H_2 is recycled. High operating pressure, typically between 100 - 250 bar [4], is used to ensure effective adsorption on the catalyst surface. Achieving such high pressures while minimizing power demand is done by having several compressors in series with the same compression ratio.

The ammonia produced in the synthesis loop will need to be cooled to subzero temperatures in order to condense, even at high pressures. How this is done in practise is explained in Section 2.2.5. This is the only method for compounds to leave the system except when the system is purged. The synthesis loop will need to be purged at regular intervals due to accumulation of inert compounds in the system. These compounds include argon, which is present in the atmosphere at approximately 0.93% [22] and enters the system with the nitrogen source. Methane also accumulates in the synthesis loop as carbon dioxide present in the nitrogen or hydrogen source is converted to methane through the methanation reaction.

2.2.4 Methanation

The methanation reaction is an important part of treating the ammonia synthesis feedstock as it is likely to contain traces of carbon dioxide. Methanation is a process in two steps, as shown in Equations 2.15 and 2.16 [10].

$$CO_2(g) + H_2(g) \rightleftharpoons CO(g) + H_2O(g) \tag{2.15}$$

$$CO(g) + 3\,H_2(g) \rightleftharpoons CH_4(g) + H_2O(g) \tag{2.16}$$

These reactions are in practice the reverse reactions in the water-gas shift reaction and steam reforming. The reason hydrogen has to be consumed to remove CO_2, is that compounds containing oxygen will poison the catalyst in the ammonia synthesis reactor. The initial step is an endothermic reaction and is usually performed over a nickel catalyst on alumina support [14] [10].

2.2.5 Refrigeration Loop

In order for a refrigeration unit to function, a concept in thermodynamics known as isentropic expansion is used. Such a process requires a compressor, a heat sink, a valve or nozzle which provides a pressure drop, and a heat source, usually the fluid which is to be cooled to sub-zero temperatures. Such a process is depicted in 2.2

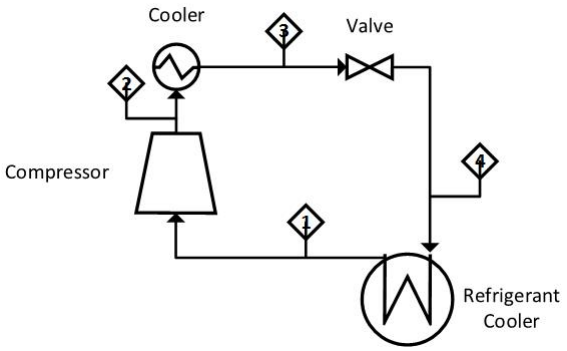

Figure 2.2: A process flow sheet for the cooling loop used in ammonia separation.

The process goes through four stages:

1. to 2. The refrigeration fluid is compressed, hence the pressure and temperature increases. The fluid remains in the gaseous state.
2. to 3. The refrigeration fluid is externally cooled. The fluid transitions into the liquid state
3. to 4. The refrigeration fluid encounters a pressure drop. Temperature drops but fluid remains mostly liquid phase.
4. to 1. The refrigeration fluid acts as a heat sink for an external fluid. The refrigeration fluid completely transitions back into the gaseous state.

These processes usually require a great deal of power to maintain, which is why refrigerant fluids are not to be used as heat sinks for streams which do not require sub-zero temperature cooling. This is why heat integration of a system is important, so to avoid the use of either refrigerants or external heating as these place a high power demand on the system.

2.3 Heat Integration

Heat integration is a method for conserving the heat generated through chemical reactions or adiabatic compression. The recovered heat can be used to heat cool streams by other means than providing external heat in the form of utility

streams. For optimal heat-recovery in a system, a heat exchanger network (HEN) is developed from a method known as pinch analysis. In pinch analysis, the most important parameter is the temperature potential difference between the hot and cold streams. This temperature, which is the minimum temperature difference between two streams which are to be matched in the HEN, ΔT_{min}, can be no less than 10 °C[19]. For the hot and cold streams to be included in the heat integration network, the temperature of each stream should be plotted as a function of enthalpy, which generates what is known as a composite curve, as shown in Figure 2.3.

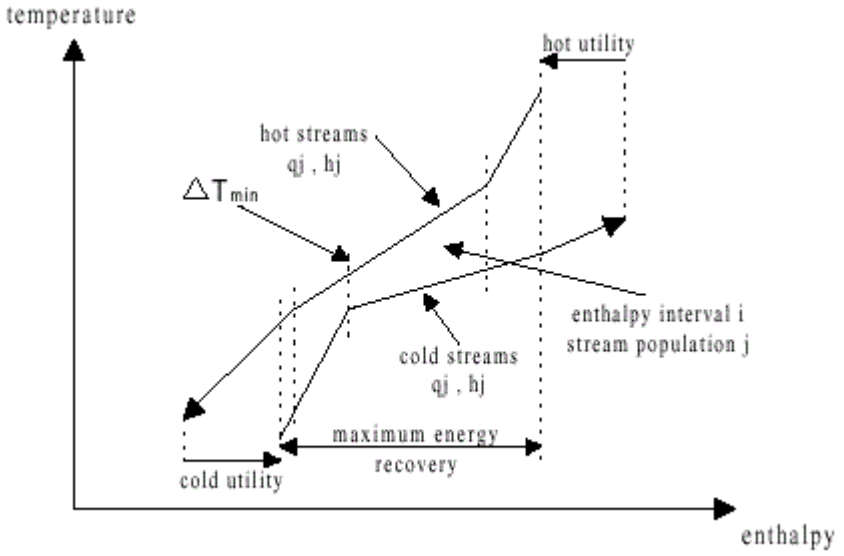

Figure 2.3: The combined hot and cold streams are plotted as a function of enthalpy.

Commonly, the minimum temperature difference, ΔT_{min}, occurs at only a single point in the composite curve and is known as the heat recovery pinch. This point divides the system into two distinct thermodynamic regions. The region above ΔT_{min} on the composite curve plot denotes the heat sink with external heat, while the region below ΔT_{min} is the heat source with external cooling. From a composite curve pertaining to a HEN, the heat recovery pinch can be discerned. Having a heat-optimal system can reduce, or even eliminate, the need for utility streams with a high power demand, but doing so could require a large heat transfer area which in turn would mean having large and heavy heat exchangers. This is not desirable on board a FPSO. Therefore, in lieu of a heat-optimal system, other parameters should be taken into account when designing a HEN for a process aboard a FPSO.

2.4 Process Design for a FPSO

The primary concern when designing a process for a FPSO are spatial limitations. Having large pieces of equipment is potentially problematic, not just because the space they require, but these components are subject to inertia, which in high seas can be a problem at best and a serious hazard at worst. Therefore, limiting the use of large pieces of equipment of great concern. However, if the sole objective is to reduce the overall size of the equipment, several other problems arise which might in certain cases take precedence over simply reducing the size. If size were the only limiting factor, having a fired heater for heating, refrigerants for cooling and maybe a couple of process-process heat exchangers would be sufficient, as seen in the Base Case HEN in Chapter 4. However, choosing such a configuration would be highly unwise as the energy required to maintain these utility streams would supersede the power capacity of the vessel for which the process is designed.

A major concern when using utility streams in offshore applications is power production and consumption. Having a single turbine to provide electricity and heating for such a large process is not a preferred situation as heaters and refrigerants require energy for continuous operation. The use of other utility streams is therefore of utmost importance. If steam could be generated by the process itself as a result of cooling a process stream, it would save a great deal of power. Readily available cooling is present in abundance in the form of cold seawater, which is disposable when it has reached a certain temperature, making it a highly viable utility stream. Utilising seawater is therefore the desired means of cooling when the temperature in the relevant process stream is too low for steam generation. In practice, seawater is not used directly. Clean cooling water, which is unlikely to cause fouling in the heat exchangers, is recycled in a loop and used to cool the process. After each loop, the heat is exchanged with seawater in a separate heat exchanger.

Hot utility streams, such as fired heated streams, should be avoided in the vicinity of oxygen-rich streams together with streams containing hydrocarbons, as they constitute a major explosion and fire hazard. Preferably, the use of HP steam should be used whenever possible when heating is required, because such streams already exist in the plant design (i.e in the pre-reforming). Also, having several different utility streams such as low pressure (LP) steam, medium pressure (MP) steam, high Pressure (HP) steam, fire heated streams, refrigerants etc. is not desirable as this would require infrastructure and piping for each individual stream. Therefore, the number of utility streams used should be as low as possible to avoid the cost of construction and maintenance of so many different streams.

Hence, when developing a heat exchanger network for the process, the above should be considered carefully when attempting to reducing the heat transfer

area (thereby reduce the overall weight of the heat exchangers) as each of the considerations will inevitably increase the required heat transfer area. Consequently, the composite curves for the hot and cold streams will be above pinch.

Chapter 3

Simulation

This chapter will present the proposed system designs, their basis, how the simulation was performed and how the process equipment were modelled. Initially, a brief explanation of the Aspen HYSYS model is given, along with the properties of the input streams and other user-defined variables. A brief outline of the properties concerning the utility streams for the process and how the heat integration was performed is given at the end of the chapter.

All simulations were conducted in Aspen HYSYS V8.6, using the Peng-Robinson fluid package. The choice of fluid package is mainly due to it being the conventional industry standard when dealing with multi-phase stream, as well as gas streams.

Operating parameters and assumptions concerning the process design were discussed and implemented in collaboration with thesis supervisor Professor Magne Hillestand and PhD candidate Mohammad Ostadi[8][16].

3.1 HYSYS Simulation of Two Proposed Designs

As set in the project outline, two different process designs were to be examined for ammonia synthesis integration into the existing GTL process design. The two process designs differ in their source of nitrogen, one utilising the N_2-rich stream in the ASU, while the other utilises the tailgas coming from the gas powered turbine used for energy production. The process flow sheet of the process design featuring the N_2-rich membrane, and the the process design featuring the tailgas are shown in Figures 3.1 and 3.2 respectively (which in this section will henceforth be referred to as design number 1 and 2 respectively). The complete simulations are given in Appendix A.

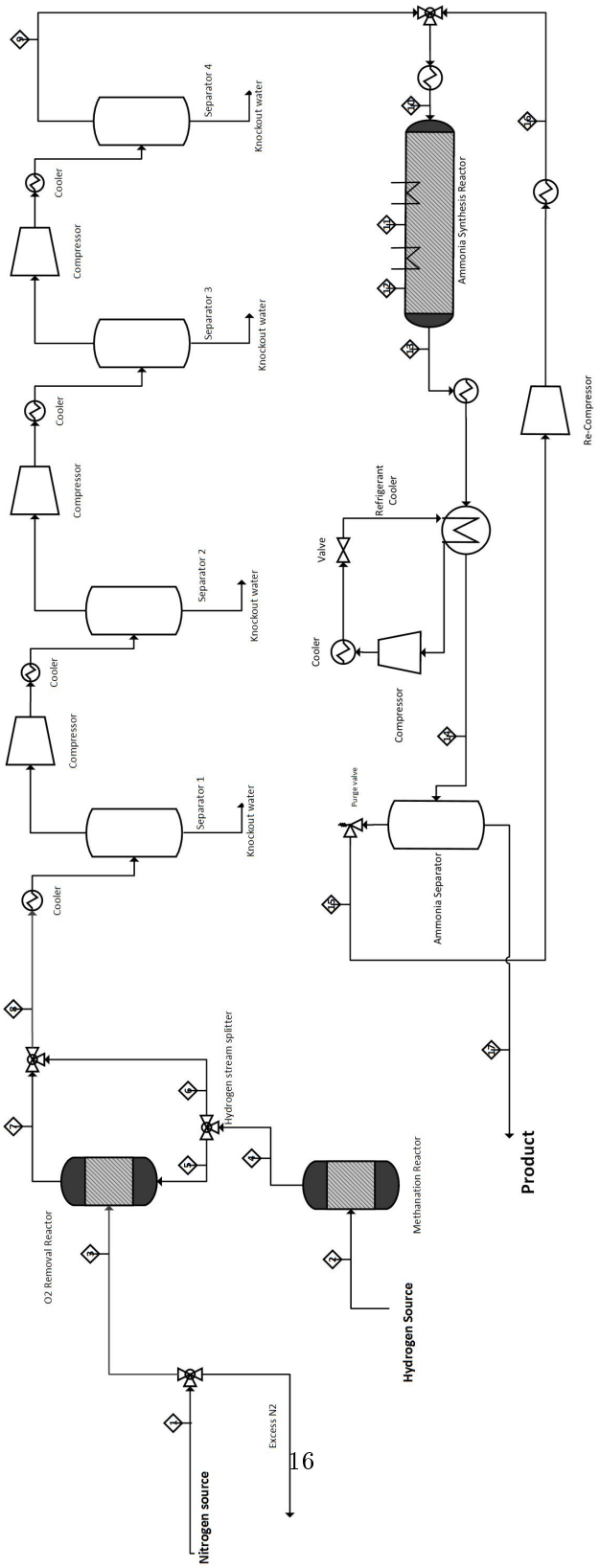

Figure 3.1: The process flow sheet for the process design when using the N_2-rich membrane stream from the ASU as the nitrogen source.

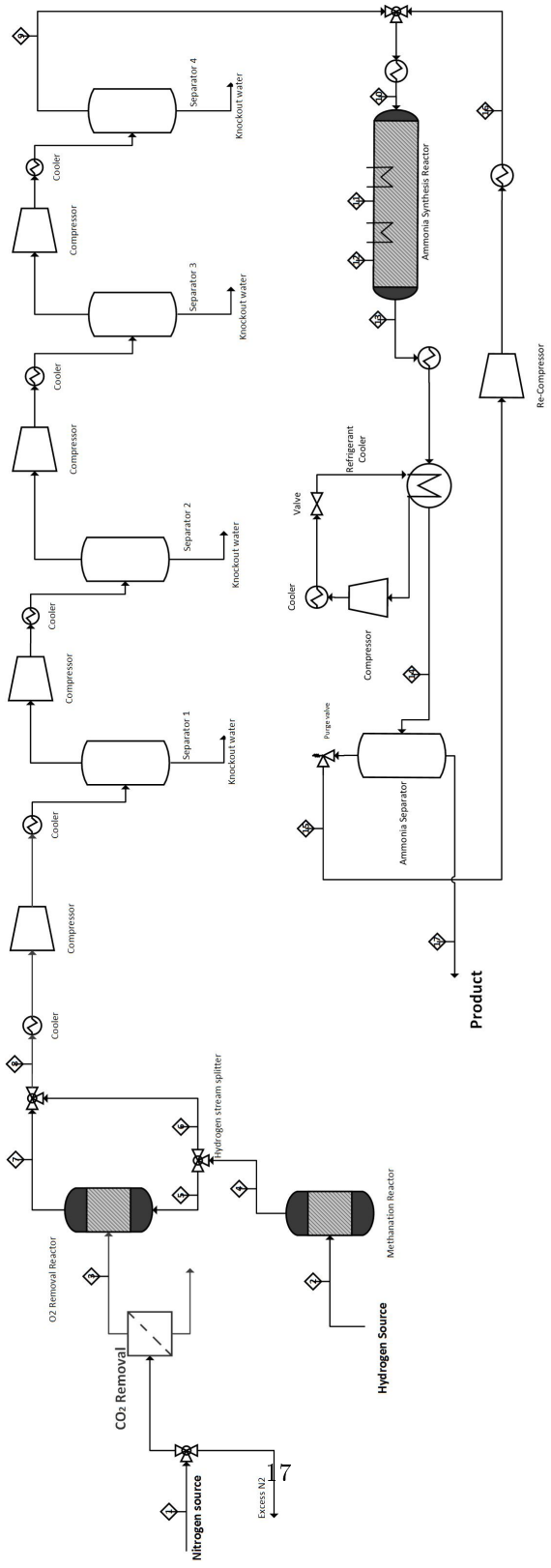

Figure 3.2: The process flow sheet for the process design featuring the tailgas from the GTL process as the nitrogen source.

3.2 Simulation Basis

In Design 1, the nitrogen is supplied by the N_2-rich stream from the ASU membrane, while in Design 2, the nitrogen is supplied by the effluent gas from the gas turbine. The nitrogen is first split to ensure a stoichiometric relationship with hydrogen at the reactor inlet. The properties of the two nitrogen sources are given in Table 3.1 for Design 1, and in Table 3.2 for Design 2.

Table 3.1: Stream properties for the N_2-rich membrane stream.

Temperature [°C]	53.5
Pressure [bar]	16.0
Molar Flow [kgmol/h]	7 869
Mole Fractions [-]	
Nitrogen	0.950
Oxygen	0.050

Table 3.2: Stream properties for the tailgas.

Temperature [°C]	385.0
Pressure [bar]	1.01
Molar Flow [kgmol/h]	28 232
Mole Fractions [-]	
Carbon-Dioxide	0.083
Nitrogen	0.809
Oxygen	0.023
Water	0.085

Design 2 differs from Design 1 in that it requires a CO_2 removal mechanism in place. Foregoing this mechanism would mean having to use the methanation reaction as discussed in Section 2.2.4 to remove the CO_2, which would be problematic for several reasons. Firstly, it would require a large amount of hydrogen to convert most of the CO_2 into methane, which in turn would mean a decrease in the theoretical amount of ammonia the design is able to produce. Secondly, a large methane presence in the stream would be problematic as the design has a synthesis loop in which vapour streams are recycled, as this would cause accumulation of methane in the system. This in turn would likely influence the conversion rate of the ammonia synthesis reactor as the accumulation of methane would lower the partial pressures of the reactive components (N_2 and H_2), subsequently reducing the conversion. A CO_2 removal process is modelled only as a component splitter, as implementing a full-scale CO_2 capture process is outside the scope of this thesis. In this simulation is assumed that 90% of the

CO_2 is removed.

The hydrogen stream, which has the same properties for each design, has the properties given in Table 3.3

Table 3.3: Stream properties for the hydrogen stream.

Temperature [°C]	213.1
Pressure [bar]	26.0
Molar Flow [kgmol/h]	1 889
Mole Fractions [-]	
Hydrogen	0.9916
Carbon Dioxide	0.0084

As given in Table 3.3, the stream contains a small amount of CO_2. The concentration in the stream is far too low for any conventional CO_2 removal mechanism however, and will have to be removed by the methanation reaction, as explained in Section 2.2.4. Due to a large partial pressure of hydrogen compared to CO_2, this is likely to result in complete conversion of CO_2, yielding a stream consisting solely of hydrogen, methane and water vapour exiting the methanation reactor.

The hydrogen stream is split with one stream going to the Oxygen Removal Reactor, while the other merges with the stream coming out of the aforementioned reactor. The Oxygen Removal Reactor is modelled as a Gibbs reactor. The reason not all of the hydrogen is sent to the Oxygen Removal Reactor, is that when temperatures rise due to the combustion, temperatures reach the point where ammonia forms spontaneously. While not initially a problem for the reactions taking place in the reactor, the resulting ammonia will likely be lost later in the process when water is removed through condensation. However, due to the reactions explained in Section 2.4, methane will react with oxygen before hydrogen is consumed, resulting in formation of CO_2. This means that the reactor requires more hydrogen to convert the resulting CO_2 back into methane. In order to deal with these effects, the hydrogen stream has to be sufficiently large in order to remove most traces of CO_2 and CO, while sufficiently small in order to prevent the unwanted formation of ammonia.

After removing all of the oxygen and CO_2, the stream now contains a fair amount of water vapour. The water is removed in a series of compressors, separators, and coolers. The streams are cooled to 20 °C before each separator, and a constant pressure ratio is used for each compressor.

When the stream enters the synthesis loop, it is heated before it enters the reactor. In lieu of implementing several beds in a single reactor, the complete

ammonia synthesis reactor was simulated as three separate reactors, each reactor representing a single bed. After exiting each bed, the stream is cooled before entering the following bed. Each bed is modelled as kinetic reaction, with two different kinetic models, which will be explained in Section 3.3. Over each bed, it is assumed a pressure drop of 5 bar.

After the stream exits the reactor, the stream is first cooled to 20 °C before being further cooled to −16 °C by the refrigeration loop, for which implementation will be explained in Section 3.4. The stream now contains a liquid fraction which will be separated out yielding a relatively pure ammonia product stream, while containing trace amounts of inert compounds. The vapour fraction is recycled, re-compressed, and re-heated to 20 °C.

The complete list of inputs is given in Table 3.4.

Table 3.4: Inputs and design parameters for the process design.

Parameter	Value
Water separation temperature [°C]	20
Maximum amount of CO_2 present in syngas stream [kgmol/h]	0.001
Maximum amount of water present in syngas stream [kgmol/h]	1.00
Reactor bed pressure drop [bar/bed]	5.00
Ammonia separation temperature [°C]	−16.00
Recycled gas re-heating [°C]	20

3.3 Kinetics

Two different kinetic models were examined, each set with a different simulation basis, and each with a different set of kinetic constants for the forward reaction, r_1, and the backward reaction, r_{-1}. Each model was simulated in Aspen HYSYS as a kinetic model.

3.3.1 Temkin-Pyzhev Kinetics

One kinetic model is the one proposed by Temkin-Pyzhev in 1960 [7]. The rate equation is given in Equation 3.1.

$$\mathrm{r_{NH_3}} = \mathrm{r_{forward}} - \mathrm{r_{backward}} = k_1 \frac{\mathrm{p_{N_2}} p_{H_2}^{1.5}}{\mathrm{p_{NH_3}}} - k_{-1} \frac{p_{NH_3}}{p_{H_2}^{1.5}} \tag{3.1}$$

For this rate equation, the pre-exponential factor, A, and the activation energy, E_a, is used to calculate the rate constants k_1 and k_{-1} expressed in the Arrhenius equation, given in Equation 3.2:

$$\mathrm{k} = \mathrm{A} \cdot \frac{\mathrm{e}^{\frac{-\mathrm{E_a}}{\mathrm{RT}}}}{\mathrm{T}} \tag{3.2}$$

For this particular rate equation, the constants are given in Table 3.5 [7].

Table 3.5: Rate Constants for the Temkin-Pyzhev equation.

	A [-]	E_a [kJ/kgmole]
k_1	17 895	87 027
k_{-1}	2.5714×10^{16}	1.9832×10^5

The remaining required settings are given in Table 3.6.

Table 3.6: Kinetic reaction settings in HYSYS for Temkin-Pyzhev kinetics .

Parameter	Setting
Basis	Partial Pressure
Base Component	Nitrogen
Reaction phase	Vapour phase
Basis Units	atm
Rate Units	$kgmole\ m^{-3}h^{-1}$

3.3.2 Langmuir-Hinshelwood Kinetics

A different approach to modelling ammonia synthesis is using the Langmuir-Hinshelwood kinetic model. It assumes that the second step in the mechanism shown in Section 2.6, the breaking of N_2 on an active site into $2N^*$, is the rate determining step. The rate expression can then be formulated as given in Equation 3.3[7]

$$r_{NH_3} = r_{forward} - r_{backward} = k_1 \phi_{N_2} - k_{-1} \frac{\phi_{NH_3}^2}{\phi_{H_2}^3} \tag{3.3}$$

The rate constants required to calculate the backwards and forwards reaction rate from Equation 3.2 and 3.3 are given in Table 3.7 [7].

Table 3.7: Rate Constants for the Langmuir-Hinshelwood equation.

	A [-]	E_a [kJ/kgmole]
k_1	1.00	1 100
k_{-1}	8.9×10^{11}	1.1×10^5

The remaining required settings are given in Table 3.8.

Table 3.8: Kinetic reaction settings in HYSYS for Langmuir-Hinshelwood kinetics.

Parameter	Setting
Basis	Fugacity
Base Component	Nitrogen
Reaction phase	-
Basis Units	atm
Rate Units	$kgmole\ m^{-3}h^{-1}$

3.4 Refrigeration Loop

As discussed in Section 2.2.5, in order to remove ammonia from the synthesis loop, it has to be cooled to sub-zero temperatures in order to condense. In this simulation, instead of dimply simulating the temperature change as a cooler, a cooling loop is simulated. An outline of the loop is shown in Figure 3.3.

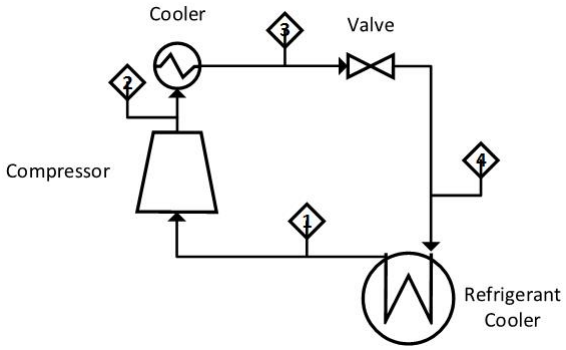

Figure 3.3: A process flow sheet for the cooling loop used in ammonia separation.

Figure 3.3 shows the four different stages in the cooling loop, as explained in Section 2.2.5. The loop was simulated such that the outlet on tube side of the heat exchanger has a fixed temperature, namely -16.00 °C. The specified variable for the refrigeration loop is given in Table 3.9. The full HYSYS simulation is given in Appendix A.

Table 3.9: Design basis for the refrigeration loop.

Parameter	Setting
Tube side outlet temperature [°C]	−16.00
Refrigeration fluid [-]	Ammonia
Pre-compression fluid pressure [bar]	1.00
Pre-compression vapour fraction [-]	1.00
Post-compression pressure [bar]	11.00
Post-compression cooling [°C]	20.00
Valve pressure drop [bar]	10.00
Shell side inlet temperature [°C]	−33.26
Vapour fraction after heat exchanger [-]	1.00

Note that the flow rate of the refrigerant fluid is not specified. This is because HYSYS detects an over-specification of variables if the properties before the recycle function used in simulation does not exactly match that of the stream that comes after it. This in principle means that the flow rate will have to be tuned so that all of the refrigeration fluid will be converted to vapour phase in the shell side of the heat exchanger before it is linked to the recycle function. This in turn makes the flow rate dependant on the heat load, which will change with the stream properties of the stream entering the tube side of the heat exchanger.

3.5 Heat Integration

The heat integration for the system was conducted in Aspen Energy Analyzer. The basis for the development of the heat exchanger network (HEN) was the HYSYS simulation of the best case scenario decided upon in Chapter 4. Aspen Energy Analyzer was used to develop a heat exchanger network to suit a process developed for off-shore applications and therefore has a few restrictions placed on it to prevent a heat optimal design as discussed in Section 2.3.

The properties of the utility streams used in the heat integration are given in Table 3.10

Table 3.10: Properties of the utility streams in Aspen Energy Analyzer.

Utility	Temperature, Inlet [°C]	Temperature, Outlet [°C]
Cold Utilities		
HP Steam	249.00	250.00
MP Steam	174.00	175.00
LP Steam	124.00	125.00
Air	30.00	35.00
Cooling Water	10.00	35.00
Hot Utilities		
LP Steam	124.00	125.00
Fired Heater	1000.0	400.00

The values in Table 3.10 are all the default values for the utility streams given by Aspen, with the exception of cooling water. The temperature is changed from 20 °C to 10 °C. The reason for this is that this process is designed for a FPSO and seawater is likely to have a lower temperature. This also provides greater driving force in the heat exchangers, resulting a in lower heat transfer area. Cooling water is therefore a cheap and effective alternative to efficient cooling when not producing steam.

After the HYSYS simulation is imported into the Energy Analyzer, the software can generate configurations given certain optimisation parameters, i.e. lowest possible area, lowest possible operational cost, etc. These generated configurations do not always offer a feasible configuration. Usually, the software will realise this by itself and flag these configurations as infeasible, but sometimes not. If the proposed configurations contain a heat exchanger with a non-specified heat transfer area, the configuration is infeasible even if it is not flagged as such by the software.

Chapter 4

Results and Discussion

The simulation of ammonia synthesis was performed as described in Chapter 3. This chapter will present and discuss the results obtained in the final process design, the background and reason for each user-defined parameter bearing an impact on the result, as well as an evaluation of the assumptions made for the system. In Section 4.1, a presentation of the two proposed designs, as set in the initial project outline, are shown with key values to determine their viability. The design which had the theoretical highest amount of ammonia produced, is the one evaluated thoroughly in Section 4.2.

4.1 Process Design

The process flow sheet of the process design featuring the N_2-rich membrane, and the process design featuring the tailgas are shown in Figures 4.1 and 4.2 respectively. The flow sheet for each process design is reproduced here, as this chapter will refer to the individual streams labelled in the process flow sheet.

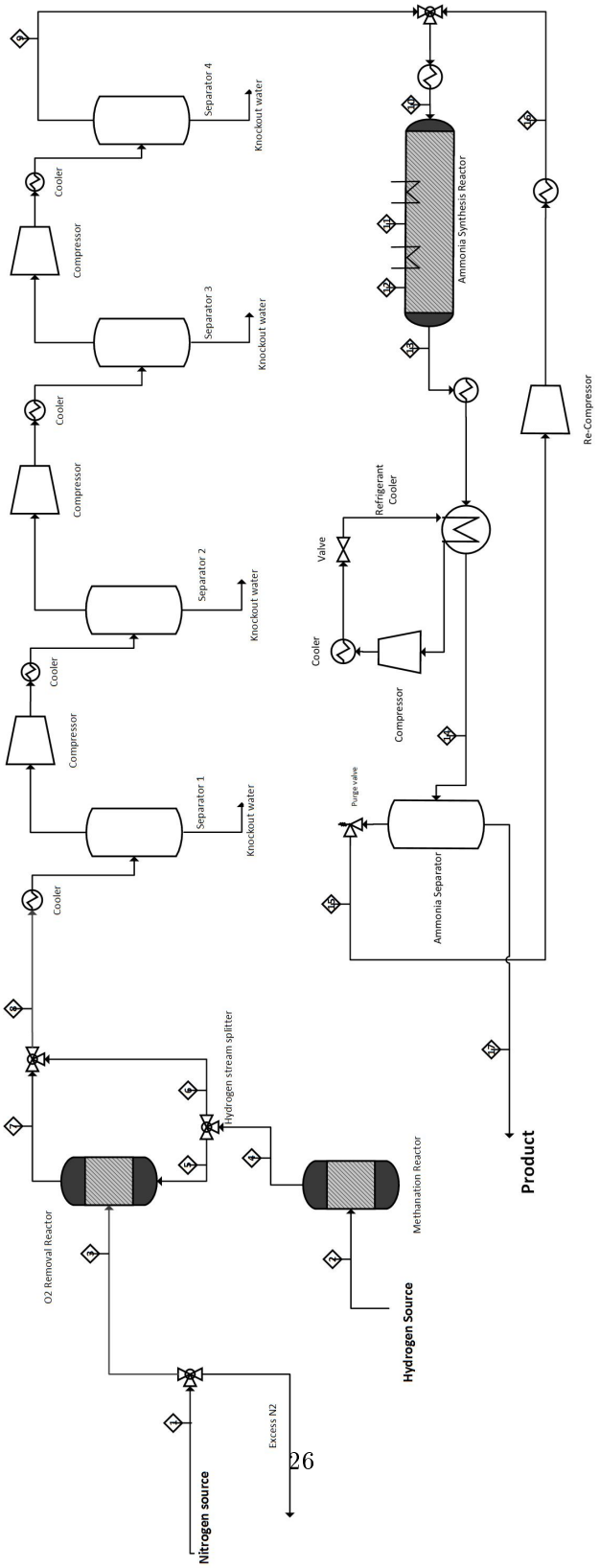

Figure 4.1: The process flow sheet for the process design when using the N_2-rich membrane stream from the ASU as the nitrogen source.

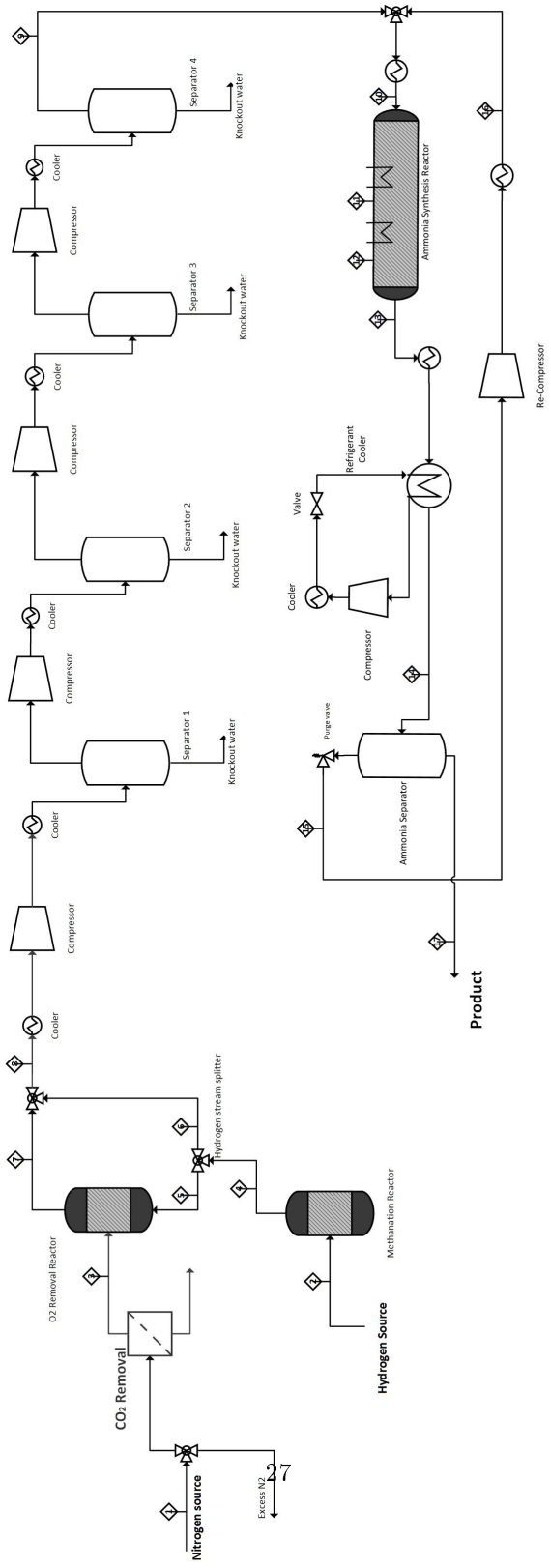

Figure 4.2: The process flow sheet for the process design featuring the tailgas from the GTL process as the nitrogen source.

As explained in Section 3.2, the fraction of the hydrogen stream which is diverted into the Oxygen Removal Reactor requires some calculation. Hence, a case study was performed to determine the split ratio of the H_2/CH_4 stream from the methanation reactor. The result is shown in Figure 4.3, and the value implemented in the simulation is given in Table 4.1. The values used for Figure 4.3 are given in Appendix D.

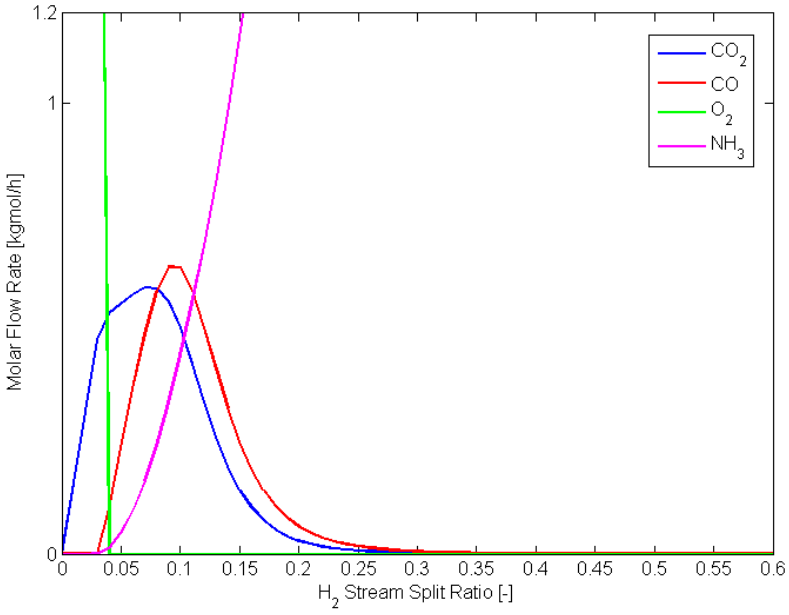

Figure 4.3: The molar flows of O_2, CO_2, CO, and NH_3 out of the Oxygen Removal Reactor as a function of the stream split ratio in hydrogen stream splitter.

Note that formation of NH_3 occurs before CO_2 and CO is completely removed. Hence NH_3 formation can only be mitigated, not prevented entirely.

A second consideration is the molar ratio between H_2 and N_2 after the water removal process. At this point, before the stream enters the ammonia synthesis loop, the ratio should be 3:1. Therefore, another case study was performed to determine the split ratio of the nitrogen stream. The result is given in Table 4.1. The values used for Table 4.1 is given in Appendix D.

Table 4.1: The split ratios for the two streams based on the calculation by performing the aforementioned case studies.

	N_2 stream	H_2 stream
Split ratio 1	0.084	0.350
Split ratio 2	0.916	0.650

Design 2 differs from the other design by having its nitrogen source containing approximately 8.3% of CO_2. The bulk of this has to be removed by a CO_2 removal process, which will not be discussed in this thesis. If this CO_2 is not removed by something other than methanation, the remaining amount of hydrogen left over for ammonia synthesis will be far too low for any meaningful comparison with Design 1. It is assumed that 90% of the CO_2 is removed after the inlet stream is split, as shown in figure 3.2. Further removal of CO_2 is done through methanation similarly to Design 1. A case study was performed to determine the split ratio accordingly, the results are shown in Figure 4.4 and the concrete split ratio is given in table 4.2. The values used for Figure 4.4 and Table 4.2 are given in Appendix D.

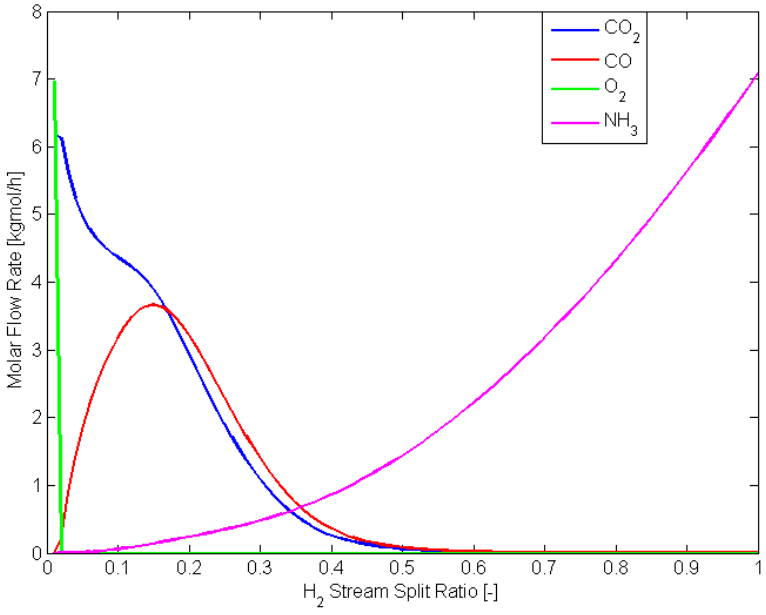

Figure 4.4: The molar flows of O_2, CO_2, CO, and NH_3 as a function of the stream split ratio in hydrogen stream splitter.

The nitrogen split ratio was calculated similarly to Design 1, and is given in table 4.2.

Table 4.2: The split ratios for the two streams based on the calculation by performing the aforementioned case studies.

	N_2 stream	H_2 stream
Split ratio 1	0.02757	0.900
Split ratio 2	0.97243	0.100

4.1.1 Preliminary Evaluation of Designs

Comparable streams in each process design are shown in 4.3 and 4.4. The stream numbers are given in Figures 3.1 and 3.2. The basis for these streams are based on the information given and calculated in Section 4.1.

Table 4.3: The temperature, pressure, molar flow and composition of the corresponding streams in the process flow sheet for Design 1. The compositions are specified in mole fractions.

Stream Number	1	2	3	4	5	6	7	8	9
Temperature [°C]	53.5	213.1	53.5	263.4	263.4	263.4	569.9	421.6	20.0
Pressure [kPa]	16 01	26 00	16 01	26 00	26 00	26 00	16 01	16 01	200 00
Molar Flow [kmol/h]	7 869	1 889	661.1	1 857	650.1	1 207	1 224	2 432	2 339
Mole Fractions [-]									
Carbon-Dioxide	0.0000	0.0084	0.0000	0.0000	0.0000	0.0000	0.0000	0.0000	0.0000
Nitrogen	0.9500	0.0000	0.9500	0.0000	0.0000	0.0000	0.4725	0.2379	0.2473
Oxygen	0.0500	0.0000	0.0500	0.0000	0.0000	0.0000	0.0000	0.0000	0.0000
Hydrogen	0.0000	0.9916	0.0000	0.9744	0.9744	0.9744	0.4571	0.7139	0.7421
Ammonia	0.0000	0.0000	0.0000	0.0000	0.0000	0.0000	0.0068	0.0034	0.0035
Water	0.0000	0.0000	0.0000	0.0171	0.0171	0.0171	0.0592	0.0383	0.0002
Methane	0.0000	0.0000	0.0000	0.0085	0.0085	0.0085	0.0000	0.0065	0.0068
Carbon-Monoxide	0.0000	0.0000	0.0000	0.0000	0.0000	0.0000	0.0045	0.0000	0.0000

Table 4.4: The temperature, pressure, molar flow and composition of the corresponding streams in the process flow sheet for Design 2. The compositions are specified in mole fractions.

Stream Number	1	2	3	4	5	6	7	8	9
Temperature [°C]	385.0	213.1	385.0	263.4	263.4	263.4	433.6	421.3	20.0
Pressure [kPa]	101.32	26 00	101.32	26 00	26 00	26 00	101.32	101.32	200 00
Molar Flow [kmol/h]	2 8232	1 889	668.0	1 857	1 672	185.7	2 306	2 491	2 354
Mole Fractions [-]									
Carbon-Dioxide	0.0834	0.0084	0.0090	0.0000	0.0000	0.0000	0.0000	0.0000	0.0000
Nitrogen	0.8091	0.0000	0.8748	0.0000	0.0000	0.0000	0.2522	0.2334	0.2470
Oxygen	0.0226	0.0000	0.0244	0.0000	0.0000	0.0000	0.0000	0.0000	0.0000
Hydrogen	0.0000	0.9916	0.0000	0.9744	0.9744	0.9744	0.6782	0.7003	0.7411
Ammonia	0.0000	0.0000	0.0000	0.0000	0.0000	0.0000	0.0024	0.0023	0.0024
Water	0.0848	0.0000	0.0917	0.0171	0.0171	0.0171	0.0583	0.0553	0.0002
Methane	0.0000	0.0000	0.0000	0.0085	0.0085	0.0085	0.0088	0.0088	0.0093
Carbon-Monoxide	0.0000	0.0000	0.0000	0.0000	0.0000	0.0000	0.0000	0.0000	0.0000

A few key features differentiate between the two designs. As seen in stream number 9 (referring to the label in Figures 3.1 and 3.2) in Tables 4.3 and 4.4, Design 1 has slightly less hydrogen compared to Design 2. This in turn, theoretically, means less ammonia produced as the amount of nitrogen present is exactly 1/3 that of hydrogen. However, as further simulation confirms, Design 2 actually produces less ammonia, and has a higher recycle ratio compared to Design 1, when the conditions in the synthesis loop are the same for both designs. This is probably due to a greater presence of inert components in Design 2, which, when they accumulate, will lower the conversion rate of N_2 and H_2 into NH_3. Design 2 also requires a CO_2 capture system in place, as well as re-pressurising the tailgas after it has exited from the gas turbine, which requires an additional compressor.

Process Design 1 is therefore the more attractive alternative and will be the alternative subject to further evaluation.

4.2 Evaluation of Kinetic Models

This section will deal with the optimisation of the ammonia synthesis loop shown in Design 1. At this point it is important to address the inherent properties of a synthesis loop. In a simulation, the system will theoretically produce roughly the same amount of product as long as the product is present in a phase where it can leave the system i.e. through condensation and separation. Hence, in the case of the ammonia synthesis loop, as long as the pressure is sufficiently high, or the temperature before the separator is sufficiently low to allow for condensation of ammonia, any physical change to the system will only have an incremental effect on the flow rate in the product stream. However, physical changes to the system will have an impact on two very important variables; the size, and power demand of the process equipment, as these are both functions of the recycle ratio. If only a small fraction of ammonia is able to leave the system, this will result in a high recycle ratio, which will cause the power demand of the system to increase. A high flow rate in the system will also influence the size required for the process equipment. The equation for the recycle ratio is given in Equation 4.1.

$$\mathrm{R} = \frac{\dot{N}_{\mathrm{Fresh}}}{\dot{N}_{\mathrm{Recycled}}} \tag{4.1}$$

4.2.1 Kinetics

The two different kinetic models presented in Section 3.3 were examined for optimal pressure and temperature for the reaction.

4.2.2 Once-through Conversion, Reactor Temperature

A simulation was run to give a preliminary examination of the once-through conversion rate of the first bed in order to estimate optimal operating temperature for the two kinetic models. The results for the Langmuir-Hinshelwood model is given in Figure 4.5, and the Temkin-Pyzhev model in Figure 4.6. The data from which the figures are based is given in Appendix D.

The simulation was run at a constant pressure of 175 bar for both cases, and specifications for the reactor were identical.

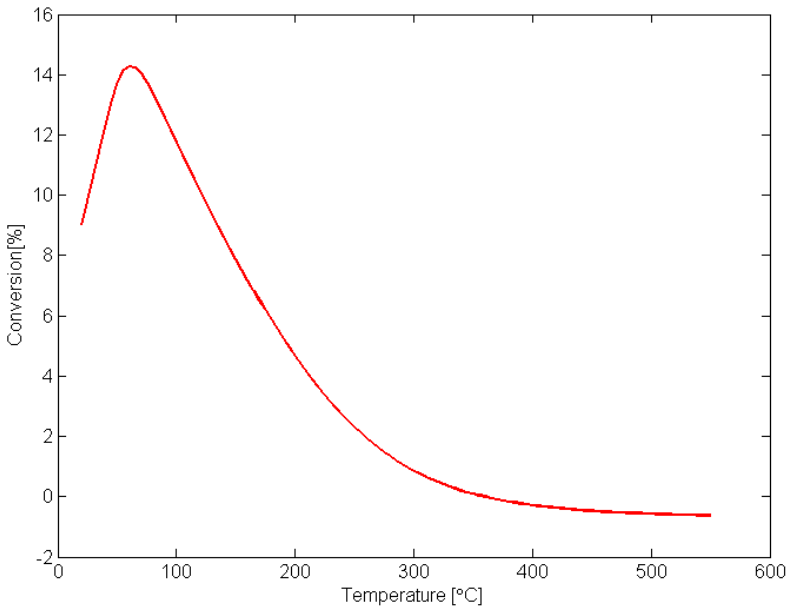

Figure 4.5: Conversion as a function of temperature for the Langmuir-Hinshelwood kinetic model.

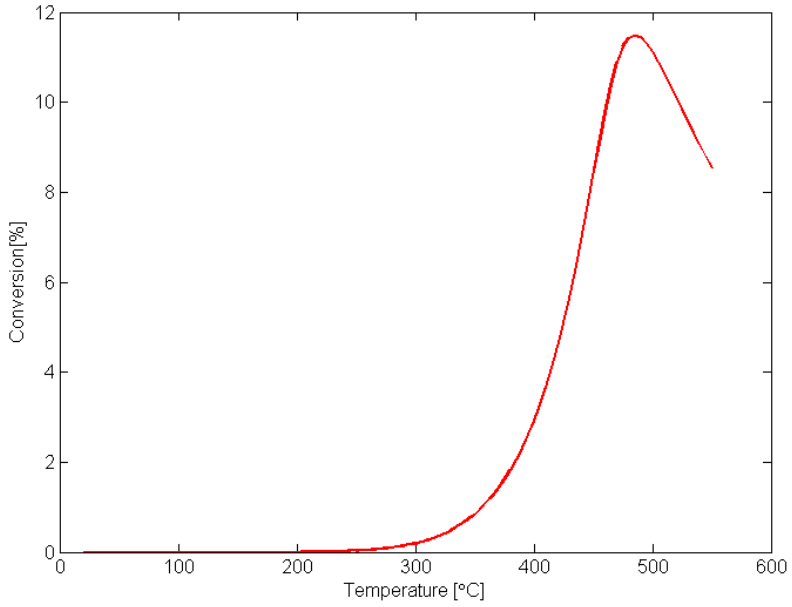

Figure 4.6: Conversion as a function of temperature for the Temkin-Pyzhev kinetic model.

From the thermodynamics in this reaction shown in Section 2.2, the reaction favours low temperatures as the reaction is exothermic. However, low temperatures will prevent adsorption of nitrogen in the catalyst, so a compromise has to be made. From Figure 4.5 it seems that the model does not account for the effect adsorption of nitrogen on the catalyst surface, as the highest conversion the reactor can reach under constant pressure is at approximately 60 °C. This conflicts with the temperature expected in conventional reactors, which is in the vicinity of 350-550 °C[4]. The values in Figure 4.6 coincide with this assumption, as maximum conversion is achieved at around 485 °C.

4.2.3 Once-through Conversion, Reactor Pressure

Each kinetic model was given a preliminary examination for optimal operating pressure. The simulation first set the temperature to the optimal temperature observed in Figures 4.5, 65.0 °C, and 4.6, 485.0 °C for the respective model. The result is given in Figures 4.7 and 4.8.

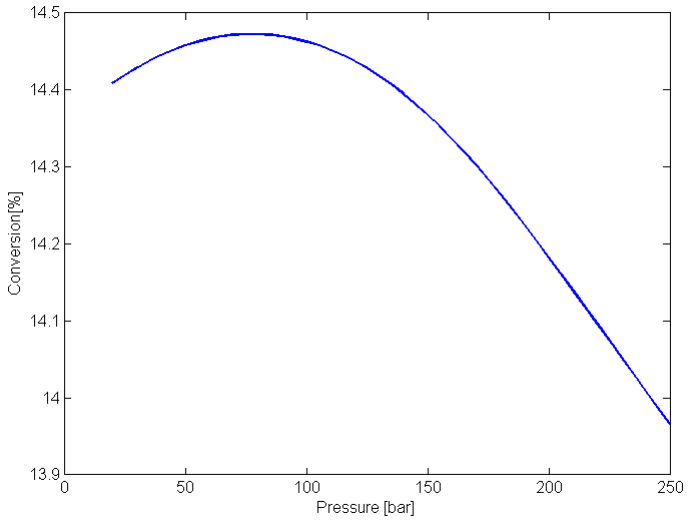

Figure 4.7: Conversion as a function of pressure for the Langmuir-Hinshelwood kinetic model with temperature kept constant at 60 °C.

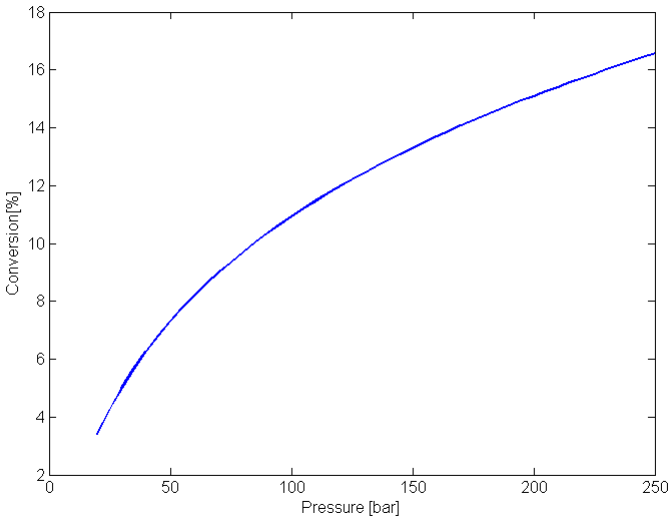

Figure 4.8: Conversion as a function of pressure for the Temkin-Pyzhev kinetic model with temperature kept constant at 480 °C.

A second simulation was conducted in which the temperature was kept constant at 275 °C for both models, which is the average of the two optimal temperatures.

The result is given in Figures 4.9 and 4.10.

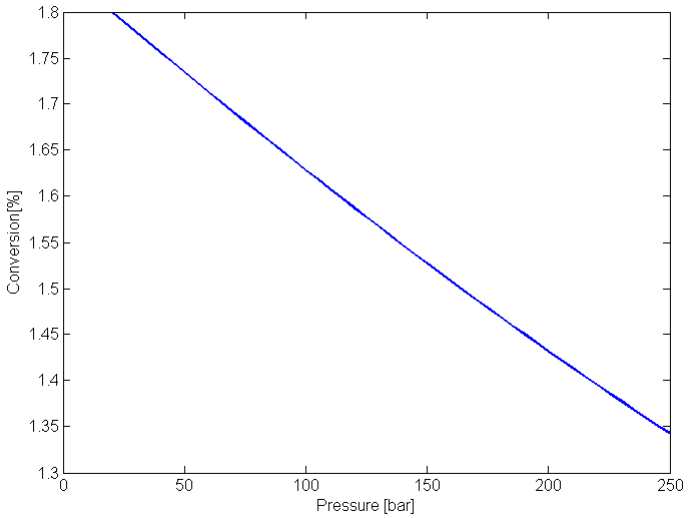

Figure 4.9: Conversion as a function of pressure for the Langmuir-Hinshelwood kinetic model with temperature kept constant at 275 °C.

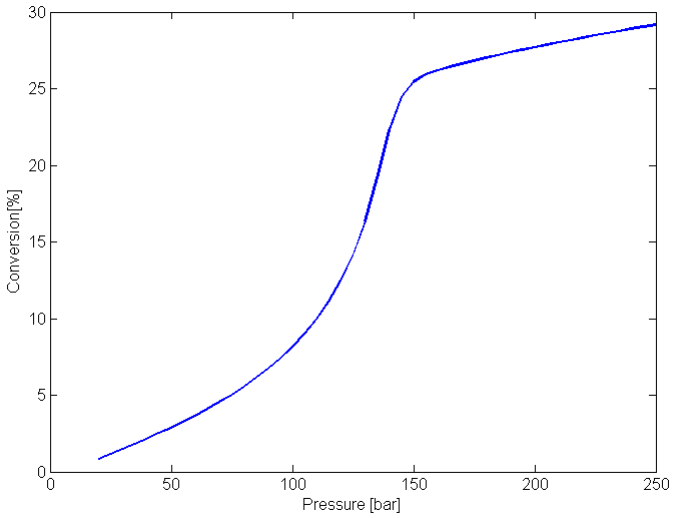

Figure 4.10: Conversion as a function of pressure for the Temkin-Pyzhev kinetic model with temperature kept constant at 275°C.

The observed conversion as a function of pressure observed in Figures 4.7 - 4.10 touches on some limitations in both kinetic models.

The Langmuir-Hinshelwood model behaves not as one would expect given the laws of thermodynamics outlined in Section 2.4. Figure 4.9 shows a linear *decrease* in conversion as pressure increases, which does not conform to expectations. When pressure increases, the expected system response is a gradual non-linear *increase* in conversion eventually reaching a horizontal asymptote, as observed in Figure 4.8. The response in Figure 4.7 is an optimal pressure at approx. 80 bar, which when compared to conventional reactors is too low [4].

The Temkin-Pyzhev model seems to correspond well with expectations with respect to pressure increase effect on the system response. While not having a clear optimal operating pressure, further investigation is required to decide on the best possible operating pressure. Figure 4.10 shows a very high conversion rate, far above what one might expect from a conventional reactor [4]. This is probably due to the nature rate equation, equation 3.1, as the partial pressure of ammonia has a negative effect on the reaction rate. In a once-through run, the only ammonia present in the system is the ammonia generated during the oxygen removal process, hence it is very low. This results in a higher conversion in a once-through run, but a lower conversion in an actual synthesis loop where ammonia is recycled and mixed with the inlet stream. This makes the Temkin-Pyzhev model highly applicable in further simulation, as it tends to accurately represent the system design.

Due to the fact that the Temkin-Pyzhev model behaves in a predictable manner and conforms to expected conventional reactor output values, the Langmuir-Hinshelwood will not be subject to further investigation.

4.3 Operational Parameter Optimisation

When optimising the design of this particular ammonia synthesis process, a very important point to address is the fact that the amount of hydrogen present in the stream before entering the synthesis loop is the limiting factor on the theoretical ammonia production. Increasing the amount of nitrogen entering the system will decrease the maximum theoretical production of ammonia, because hydrogen will be consumed in the Oxygen Removal Reactor when removing the oxygen present in the nitrogen source, as observed in Figure 4.11.

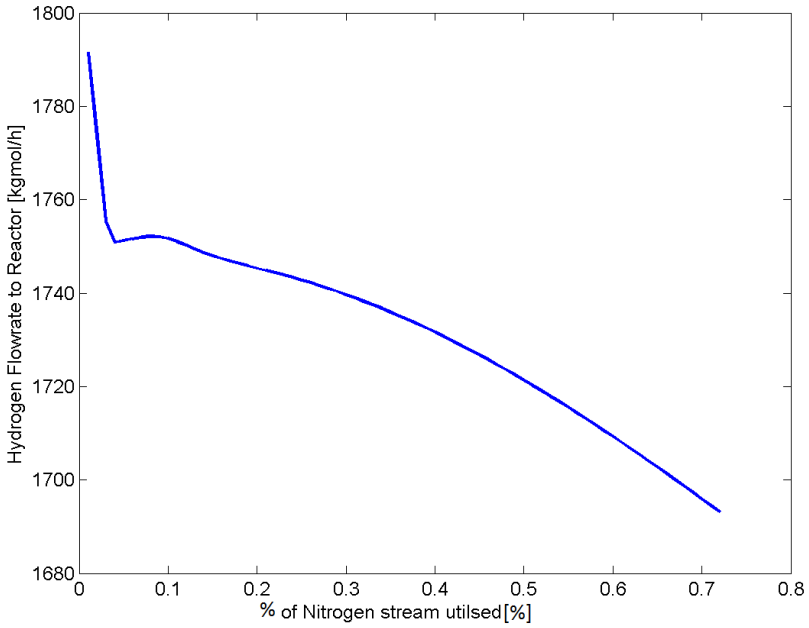

Figure 4.11: The effect on hydrogen flow to the reactor if the intake from the nitrogen source is increased.

The amount of nitrogen entering the system will therefore not exceed the amount required to maintain a stoichiometric relationship between hydrogen and nitrogen in the stream entering the synthesis loop as this will have a negative effect on the production capabilities of the system. Optimising the system with respect to nitrogen intake will therefore not be performed.

As mentioned earlier in the section, when simulation is conducted in the ammonia synthesis loop the result is a steady-state solution, which means that any changes which does not prevent ammonia from condensing has no significant impact on the product flow rate. However, the pressure in the synthesis loop, inlet temperature to each bed, reactor dimensions and other specifications all have an impact on the recycle ratio in the system.

4.3.1 Reactor Pressure in Ammonia Synthesis Loop

Different operational pressures were simulated and the effect on the synthesis loop was observed.

In Figure 4.12, the combined duty of all compressors are plotted as a function of the operating pressure for the synthesis loop. This includes the three

compressors before the synthesis loop, all of which maintain the same compression ratio, the compressor in the refrigeration loop, and the re-compression compressor in the loop. The temperature is kept constant at 480 °C.

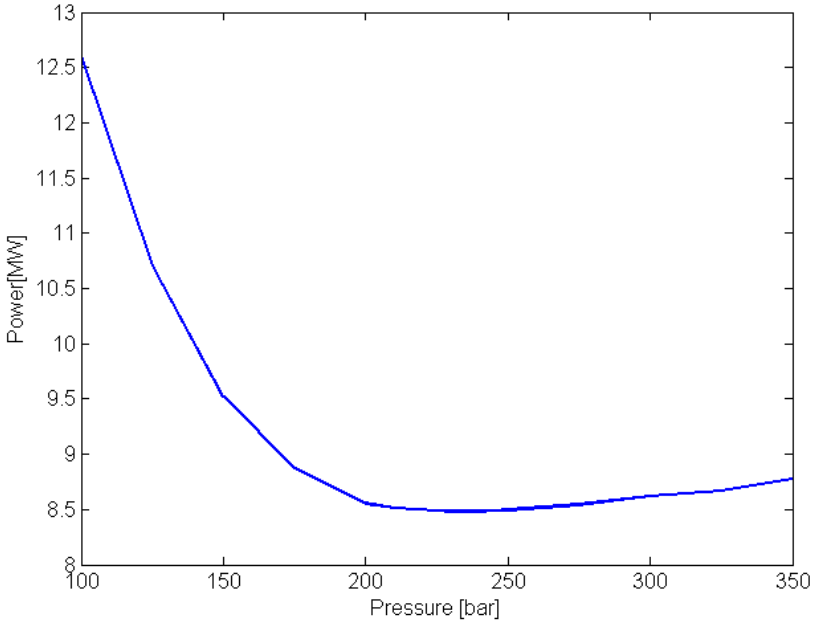

Figure 4.12: Power consumption as a function of operating pressure in the synthesis loop with temperature kept constant at 480 °C.

Figure 4.12 has two key properties. Firstly, power consumption decreases with increasing operating pressure in the synthesis loop. This is to be expected, as when observed in Section 4.2.3, higher pressure gave a higher once-through conversion. This would then result in a lower recycle ratio. What is *not* inherent from the previous simulations is that the power would increase again after a certain point.

This point exists because the duty of either the re-compression compressor, or the refrigeration loop compressor is not linearly correlated with the duty of the compressors outside the loop. This means that the point is the local minima, and possibly the global minima, as the power consumption function could likely be represented by a third degree polynomial. The power consumption as function of operating pressure for the compressors are shown in Figure 4.13.

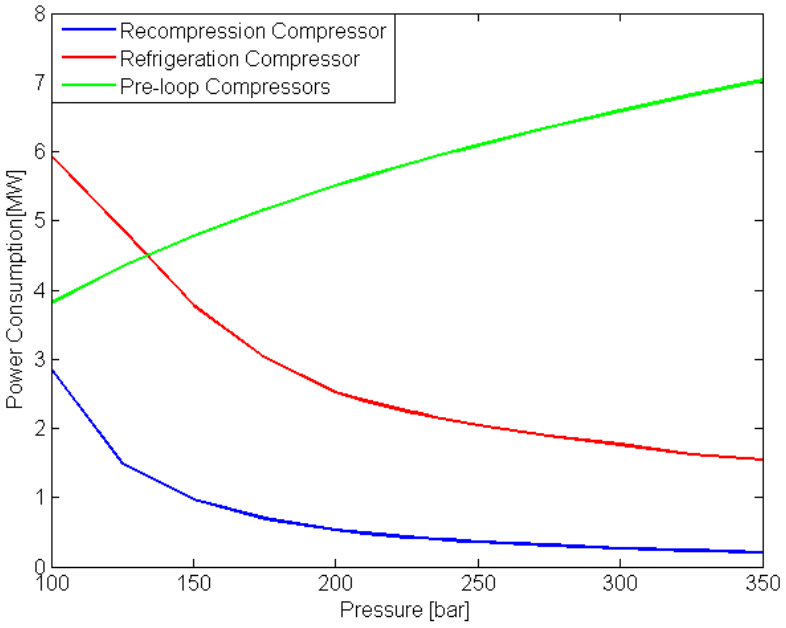

Figure 4.13: Compressor power consumption as a function of operating pressure.

As observed in Figure 4.13, the pre-loop compressors require less power as pressure increases, while the power consumption of the compressors in the loop decrease far more rapidly as pressure increases. This is because the increased operating pressure reduces the recycle ratio as more ammonia will condense at a constant temperature of -16 °C.

This is of great importance as it means that the system has a power-optimal operating pressure, which from Figure 4.12, and from the data given in Table D.10 in Appendix D, places it close to 235 bar. This pressure is also within limits of the pressure range used in commercial reactors [4].

4.3.2 Reactor Temperature

The inlet temperature to each bed was simulated using a constant operating pressure of 235 bar which was found to be the power-optimal operating pressure as discussed in Section 4.3.1. The conversion rate as a function of temperature is given in Figures 4.14, 4.15 and 4.16 for reaction beds 1, 2 and 3 respectively. The simulation data for the Figures 4.14, 4.15 and 4.16 are given in Appendix D.

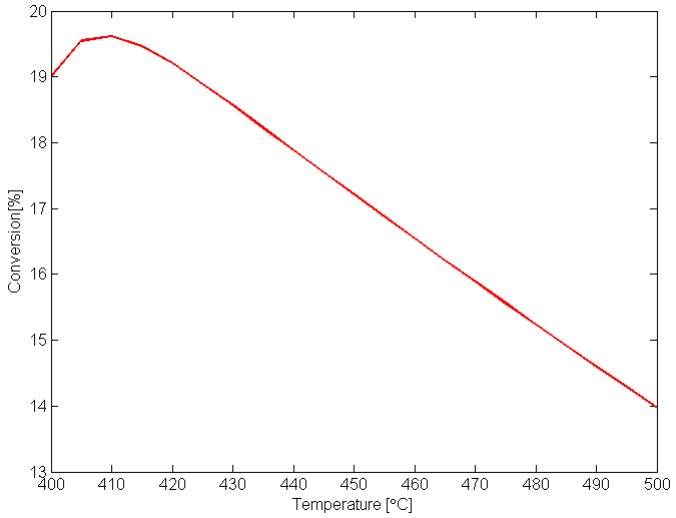

Figure 4.14: Conversion as a function of inlet temperature for Bed 1.

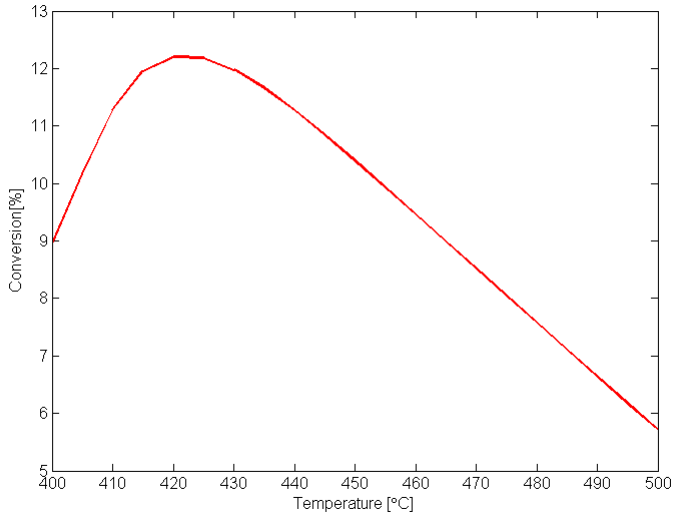

Figure 4.15: Conversion as a function of inlet temperature for Bed 2.

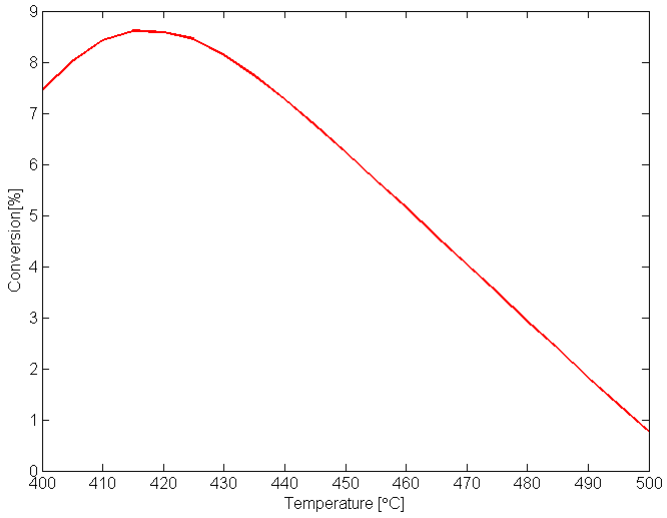

Figure 4.16: Conversion as a function of inlet temperature for Bed 3.

From Figures 4.14, 4.15 and 4.16, the optimal operating temperature can be discerned. The result is given in Table 4.5

Table 4.5: Optimal temperature at reactor bed inlet for Bed 1-3.

Bed Number	Optimal Operating Temperature [°C]
Bed 1	410
Bed 2	420
Bed 3	415

4.3.3 Reactor Bed Sizing

In order to ensure optimal operation, each reactor was sized with respect to dimensions of each bed, and the void fraction for each bed. This was to ensure reaction equilibrium, and hence maximum conversion, was reached with each pass-through. The results are given in Table 4.6 and the temperature curves showing temperature equilibrium in each bed is shown in Appendix D.

Table 4.6: Reactor Bed parameters before and after optimisation.

Before Optimisation	All Beds		
Reactor Bed Volume [m^3]	50.00		
Reactor Bed Length [m]	7.074		
Reactor Bed Diameter [m]	3.00		
Void Fraction [-]	0.5		

After Optimisation	Bed 1	Bed 2	Bed 3
Reactor Bed Volume [m^3]	8.00	31.00	45.00
Reactor Bed Length [m]	1.132	4.386	6.366
Reactor Bed Diameter [m]	3.00	3.00	3.00
Void Fraction [-]	0.6	0.6	0.85

4.3.4 Cooling Loop

The cooling loop was adjusted to meet the requirements outlined in 2.2.5 with respect to temperatures and phase changes of the refrigerant fluid. The results for the demand on the cooling system after optimisation are given in Table 4.7 to be used in conjunction with Table 3.9 in Section 3.4.

Table 4.7: Specifications for the cooling loop.

Refrigerant Flow [kgmol/h]	661.6
Compressor Duty [kW]	1 541
Cooling Duty[kW]	5 123

4.3.5 Ammonia Condensation and Separation

With the optimisation performed in Section 4.3.1 through 4.3.4, the final liquid stream from the ammonia separator had the properties presented in Table 4.8

Table 4.8: Properties and composition of the product stream.

Temperature [C]	-16.00
Pressure [kPa]	220 00
Molar Flow [kgmole/h]	1 193
Mass Flow [kg/h]	20 223
Recycle Ratio []-]	
Molar Fractions	
Nitrogen	0.0019
Hydrogen	0.0057
Ammonia	0.9780
Water	0.0004
Methane	0.0140

The values in Table 4.8 corresponds to a production rate of ammonia at approximately 19.9 tonne/h with 98.25% purity.

4.3.6 Hydrogen Efficiency

The hydrogen efficiency was calculated for the process. The hydrogen efficiency is defined as the amount of hydrogen in the product divided by the amount of hydrogen entering the system. The result is given in Figure 4.17. The calculation of the hydrogen efficiency is given in Appendix C.4.

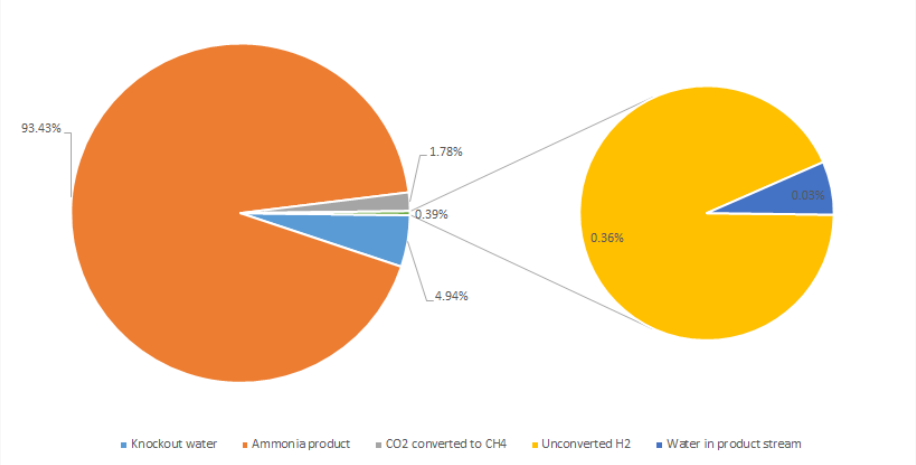

Figure 4.17: A sector diagram of where the hydrogen entering the system ends up.

From Figure 4.17, the hydrogen efficiency is found to be 93.43% with most of the lost hydrogen going towards removing the oxygen in the nitrogen source, and

from methanation removal of CO_2 and lost as knockout water. The hydrogen efficiency is difficult to compare to industry benchmarks, as the reforming of natural gas to produce the necessary hydrogen produce significant amounts of knockout water, which will decrease the over hydrogen efficiency for the process. The estimate of hydrogen efficiency of 93.43% is likely av overestimation of the efficiency for the overall process.

4.4 Heat Integration and Energy Demand

The streams requiring external heating or cooling are given in Table 4.9. Note that this does not include the stream before and after the heat exchanger connected to the cooling loop. The name of the streams in Table 4.9 corresponds to the stream names in the simulation, given in Appendix A.

Table 4.9: Stream inlet, outlet and overall temperature change in streams requiring external cooling or heating.

Cold Streams	T_{in} [°C]	T_{out} [°C]	ΔT [°C]
Recompressed_vapour_To_Reintroduced_vapour	-9.6	20.0	29.6
10_To_Reactor_in	19.8	410	390.2

Hot Streams	T_{in} [°C]	T_{out} [°C]	ΔT [°C]
Bed_2_out_To_Bed_2_cool	503.9	415	-88.9
3_To_4	421.6	20.0	-401.6
Bed_3_out_To_Reactor_out	471.1	20.0	-487.1
7_2_To_8	120.9	20.0	-100.9
8_2_To_9	121.1	20.0	-101.1
6_To_7	120.6	20.0	-100.6
Bed_1_out_To_Bed_1_cool	563.9	420	-143.9

For the Heat Integration (HI) for the system, a proposed HEN was generated in Aspen Energy Analyzer. The basis for developing the HEN was the simulation file with all optimisation done in Section 4.3 implemented. The utility streams were defined as explained in Section 3.5. One important fact to note is that process stream splitting is forbidden. Allowing stream splitting would likely yield a more heat-optimal configuration, but also a far more intricate network which would be unnecessarily difficult to implement in offshore applications. The Base Case generated is given in Figure 4.18. The values pertaining to the HEN is given in Appendix E.1.

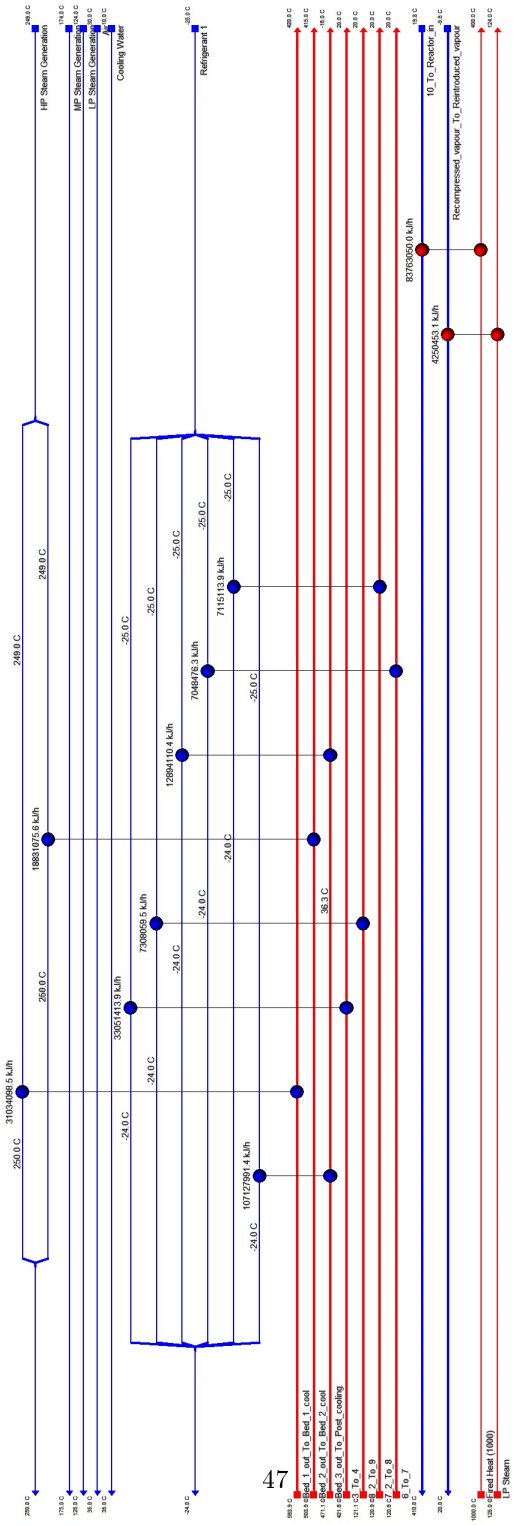

Figure 4.18: Proposed Base Case heat exchanger network.

This design is not viable as a configuration because of heavy reliance on utility streams with high energy demand, such as a fired heater and use of refrigerant. Specifications for each heat exchanger part of the HEN is given in Appendix E.1.

Aspen Energy Analyzer was used to generate 100 configurations, and the best 10 configurations are given in Appendix E.1. The best case scenario was Design 7, shown i Figure 4.19.

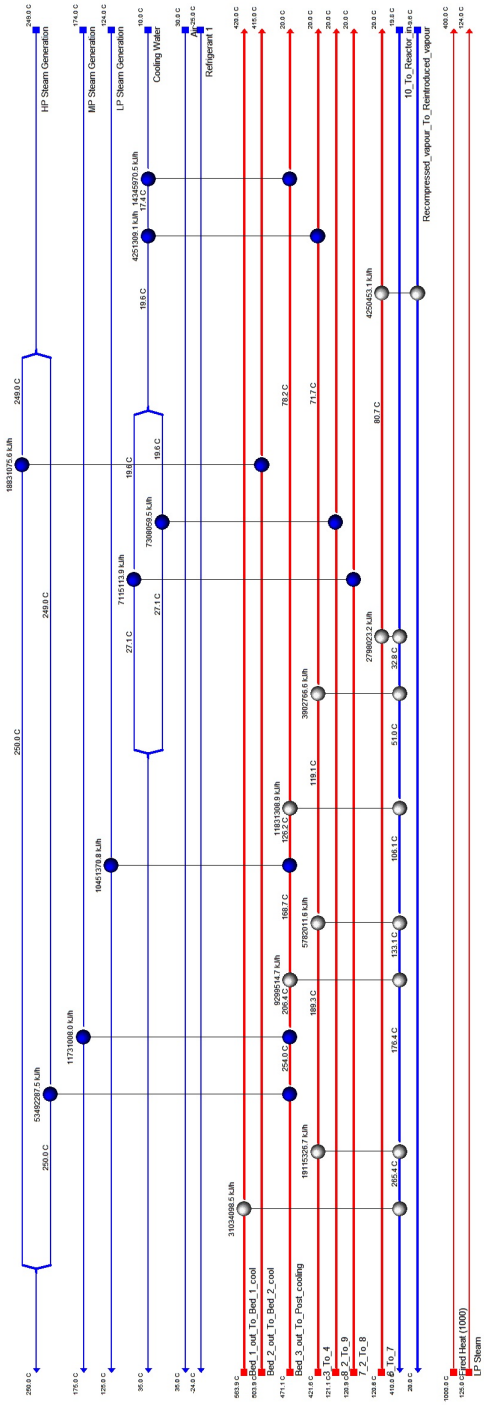

Figure 4.19: Proposed design for heat exchanger network (Design 7).

The specifications for each heat exchanger is given in Tables 4.10 and 4.11.

Table 4.10: Operational parameters for the HEN in Design 7.

Heat exchanger	Type of heat exchange	Load [kJ/h]	Area [m^2]	Shells
E-104	Process-Process	31,034,098	175.8	1
E-105	Cold Utility	18,831,076	41.5	1
E-106	Cold Utility	53,492,287	234.8	2
E-107	Process-Process	19,115,327	308.7	3
E-108	Cold Utility	11,731,008	56.1	1
E-109	Process-Process	9,299,515	189.9	2
E-110	Process-Process	5,782,012	182.1	2
E-111	Cold Utility	10,451,371	190.4	2
E-112	Process-Process	11,831,309	336.8	3
E-113	Process-Process	3,902,767	61.9	1
E-114	Cold Utility	7,115,114	269.6	4
E-115	Cold Utility	7,308,060	188.7	4
E-116	Process-Process	2,798,023	45.3	1
E-117	Cold Utility	4,251,309	139.7	2
E-118	Process-Process	4,250,453	135.0	2
E-119	Cold Utility	14,345,971	153.4	2

This design has many desirable features, most important of which is that it does not require any external heating or refrigerants. It is not heat-optimal however, as a lot of heat is wasted on cooling water in order to avoid large heat exchangers for steam production. This can be observed in the composite curve, given in Figure 4.20, which is well above pinch.

Table 4.11: Operational parameters for the HEN in Design 7.

Heat exchanger	Hot stream	T_{in}	T_{out}	Cold Stream	T_{in}	T_{out}
E-104	Bed_1_out_To _Bed_1_cool	563.9	420.0	10_To_Reactor_in	265.4	410.0
E-105	Bed_2_out_To_Bed_2_cool	503.9	415.0	HP Steam Generation	249.0	250.0
E-106	Bed_3_out_To_Post_cooling	471.1	254.0	HP Steam Generation	249.0	250.0
E-107	3_To_4	421.6	189.3	10_To_Reactor_in	176.4	265.4
E-108	Bed_3_out_To_Post_cooling	254.0	206.4	MP Steam Generation	174.0	175.0
E-109	Bed_3_out_To_Post_cooling	206.4	168.7	10_To_Reactor_in	133.1	176.4
E-110	3_To_4	189.3	119.1	10_To_Reactor_in	106.1	133.1
E-111	Bed_3_out_To_Post_cooling	168.7	126.2	LP Steam Generation	124.0	125.0
E-112	Bed_3_out_To_Post_cooling	126.2	78.22	10_To_Reactor_in	51.0	106.1
E-113	3_To_4	119.1	71.66	10_To_Reactor_in	32.8	51.0
E-114	7_2_To_8	120.9	20.00	Cooling Water	19.6	27.1
E-115	8_2_To_9	121.1	20.00	Cooling Water	19.6	27.1
E-116	6_To_7	120.6	80.69	10_To_Reactor_in	19.8	32.8
E-117	3_To_4	71.7	20.00	Cooling Water	17.4	19.6
E-118	6_To_7	80.7	20.00	Recompressed_vapour_To Reintroduced_vapour	-9.6	20.0
E-119	Bed_3_out_To_Post_cooling	78.2	20.00	Cooling Water	10.0	17.4

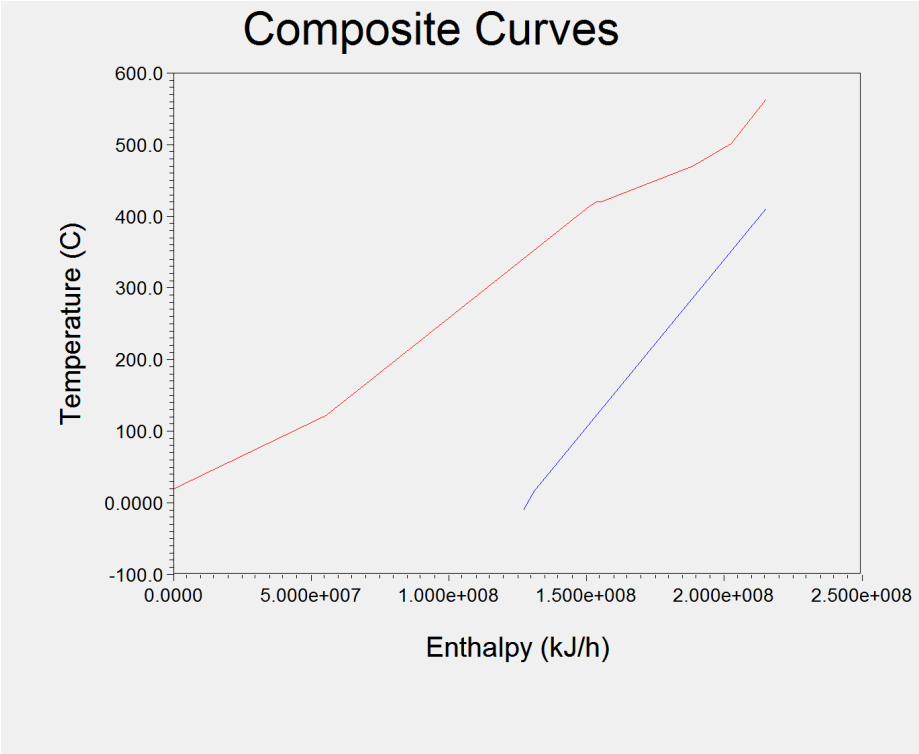

Figure 4.20: The composite curve for Design 7.

The difference in energy demand between with a process design HI and one without HI is given in Table 4.12.

Table 4.12: A comparison of energy demand for the system including and excluding heat integration (HI).

	Without HI	With HI
Cooling Demand [MW]	63.9	39.7
Heating Demand [MW]	24.5	0

4.4.1 Steam Generation

As the system produces more heat through chemical reactions than that which is consumed by heating streams in the system, the surplus energy can be used to produce steam at various pressures. The steam has no specific use in the simulation, as the compressors in the process are assumed to be electrically driven. However, these compressors could be replaced by steam driven turbines as is the industry convention [4][7]. The water used to produce steam is produced

in the four separators before the synthesis-loop. The streams are also available at increasing pressure, which makes them optimal for steam generation. The contribution of each separator is given in Table 4.13.

Table 4.13: Water available for steam production.

Separator Name	Flow Rate [kg/h]
Water Separator 1	1610.5
Water Separator 2	36.4
Water Separator 3	14.7
Water Separator 4	5.7
Total	1667.3

4.4.2 Energy Efficiency

The energy efficiency for the process after it was heat integrated was calculated as explained in Appendix C.4. The efficiency factor for the system is defined differently on a case-by-case basis, but for this particular process it is defined as the amount of energy entering the system subtracted by the energy leaving the system, and divided by the energy entering the system. The percentage of energy for each stream given in Table 4.14 is the energy of that stream divided by the total energy entering the system.

Table 4.14: An overview of where the energy entering the system ends up.

Stream	Energy percentage [%]
Ammonia product	31.80%
HP Steam	28.33%
MP Steam	4.60%
LP Steam	4.09%
Energy lost	31.18%

As can be discerned from Table 4.14, 31.8% of the total energy input ends up as ammonia, while 31.18% of the energy is lost as knockout water, through the use of cooling water and other components in the product stream apart from ammonia as explained in Appendix C.4. 37.02% of the energy is used for steam production, the bulk of it being used for HP steam production. A sector diagram presenting each component is given in Figure 4.21.

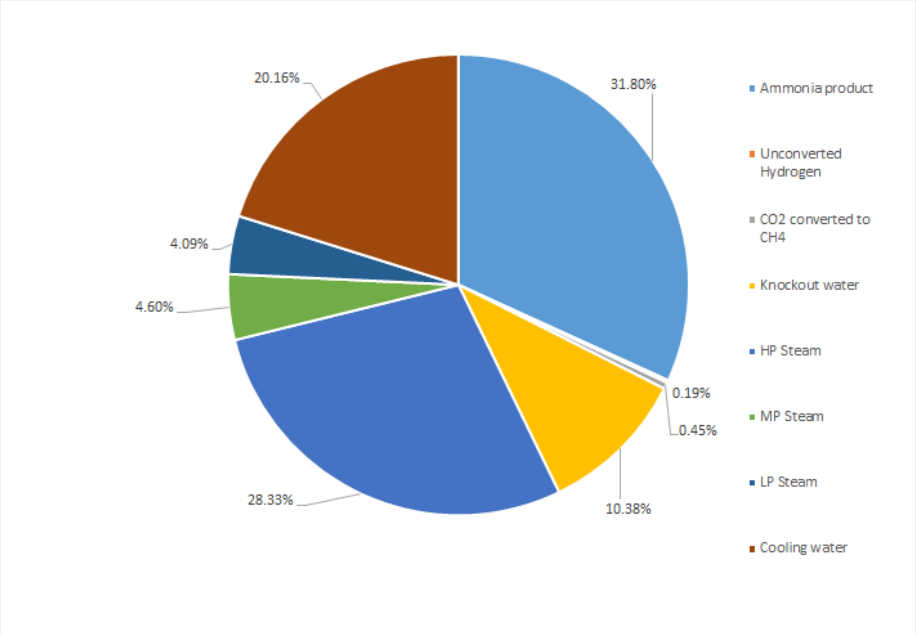

Figure 4.21: A sector diagram of where the energy entering the system ends up.

The overall efficiency of the process is therefore calculated to be 68.82%. It is not possible to compare this figure to any industry benchmarks, because this process does not include many of the process steps in conventional ammonia synthesis plants, such as air enrichment, natural gas reforming etc.

4.4.3 Power Consumption

The GTL process from which the ammonia synthesis process gets its feedstock employs a gas turbine for power production on board the FPSO. After all power sinks in the GTL process and the ammonia synthesis process are accounted for, the net power consumption and production can be calculated. The result is given in Table 4.15.

Table 4.15: Power consumption and production for the combined GTL and ammonia process.

Power Sinks		Power [MW]
GTL Process	Air compression to process	90.4
	Air compression to turbine	49.1
	H_2 compression	3.0
	CO_2 recycle compression	0.20
Ammonia Process	Pre-Loop compression	5.93
	Refrigeration compressor	1.54
	Loop re-compression	0.25
Power source	Gas turbine	179.0
Excess power		28.6

From Table 4.15, it is clear that the power production done by the gas turbine is more than sufficient to meet the additional power demand placed on it by the ammonia synthesis process.

4.4.4 Scaling

When scaling this process design, there is a linear relationship between the intake of hydrogen and nitrogen, and the production of ammonia as long as the stoichiometric relationship between hydrogen and nitrogen is maintained. As observed in Figure 4.22, which depicts the production of ammonia as a function of the molar flow of syngas with a stoichiometric relationship between hydrogen and nitrogen.

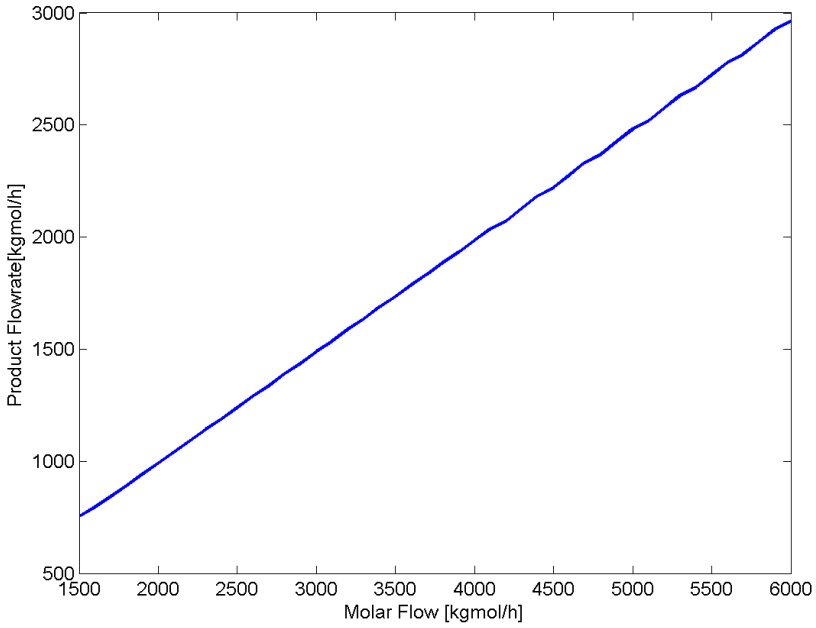

Figure 4.22: The effect on hydrogen flow to the reactor if the intake from the nitrogen source is increased

If the stoichiometric relationship is not maintained, then a build-up of the over-represented component will occur and will have to be purged from the system after a certain time of operation. Purging of the system will have to be performed at regular intervals anyway, as inert components, such as atmospheric argon, will accumulate in the system over time. However, if the stoichiometric relationship between hydrogen and nitrogen is not maintained, purging the system will have to be performed at much shorter time intervals.

4.4.5 Ammonia Synthesis As Part of the GTL Process

Evaluating the intake of natural gas flow rate and composition and its effect on the GTL and ammonia synthesis process, heat integration of the ammonia synthesis process with the GTL process, and complete economic evaluation of the production units and their products could not be performed.

This was due to the FTS reactor model made in ACM by Ostadi[16] failed to converge when the simulated values deviated too far from the initial predicted values. When a reactor model is programmed in ACM, the script requires some initial values for the user defined variables. As the model fails to converge if the simulated variables deviate from the initial predicted variables, it gives the

ACM model a very narrow set of values the model can simulate. Therefore any meaningful change to the system which would impact the nitrogen and hydrogen source could not be simulated with the current ACM model.

4.5 Equipment Sizing

Equipment sizing was performed for the ammonia synthesis process. A detailed calculation for the different equipment are given in Appendix F.0.4. Stainless steel with a density of 8 000 kg/m^3 is the assumed construction material for all equipment. The result it given in Table 4.16.

Table 4.16: Dimensions of the process equipment required for the ammonia synthesis process. Length, height and volume corresponds to the outer dimensions of each vessel.

Name	Diameter [m]	Height/length [m]	Volume [m^3]
Water Separator 1	1.18	2.42	2.88
Water Separator 2	0.96	1.84	1.48
Water Separator 3	0.81	1.59	0.93
Water Separator 4	0.73	1.44	0.73
Ammonia Separator	1.04	9.04	7.9
Oxygen Removal Reactor	2.00	3.37	11.8
Ammonia Synthesis Reactor	4.43	13.0	245.3
Methanation Reactor	0.8289	1.23	0.76

4.6 Cost Estimation

Cost estimation was performed for the equipment used in the ammonia synthesis process, and the result is given in Table 4.17. The cost estimated is the purchase cost, and does not include installation. For the ammonia synthesis reactor and the methanation reactor, the catalyst cost is included. Full and detailed calculations for the cost of the equipment are given in Appendix G.0.5.

Table 4.17: A cost estimation for the equipment pertaining to the ammonia synthesis process

Equipment	Cost [US$]
Compressors	1 827 417
Heat Exchangers	810 641
Separators	334 785
Oxygen Removal Reactor	126 753
Methanation Reactor	31 641
Ammonia Synthesis Reactor	14 144 217
Total	17 275 453

The ammonia synthesis reactor accounts for 81.9% of the total equipment cost, which is unsurprising. In a conventional ammonia synthesis plant, large parts of the equipment costs include an ASU, membrane units, a hydrogen production unit, and heat exchangers and compressors to accompany these units. In this ammonia synthesis process design, both the nitrogen stream and the hydrogen stream are readily available, and require very little treatment before being suitable for ammonia production.

The total fixed capital cost, which is the complete installation cost of the equipment, is used to calculate working capital, ISBL, OSBL and the total capital investment cost. The working capital, which is the cost needed to start up and run the process before it can produce its own income is set at 15% of the fixed investment cost. The total capital investment cost is the sum of the total fixed capital and the working capital. The results are given in Table 4.18.

Table 4.18: The total capital investment cost for the process

Cost	[Million US$]
Total Fixed Capital	76.2
Working Capital	11.4
ISBL	42.3
OSBL	33.9
Total capital investment	87.6

Chapter 5

Conclusion and Recomendations

In this master thesis, an ammonia synthesis process in conjunction with a GTL process for offshore applications was investigated. The process was successfully simulated in Aspen HYSYS V. 8.6.

Based on the two different possible sources of nitrogen, and two different set of kinetic models, it was found that:

- Using the tailgas as the source of nitrogen for ammonia synthesis was not a viable option. This was mainly because the stream is only available after it has been de-pressurised in the gas turbine and it requires a more intricate process design, including an additional compressor and a CO_2 capture system.
- The nitrogen-rich membrane stream from the ASU was the preferable option as only 8.1% of the hydrogen was consumed to treat the nitrogen stream, and the process design was relatively simple.
- The Langmuir-Hinshelwood kinetic model for ammonia synthesis was discarded. After investigation it was found that system response to varying temperatures and pressures did not conform to expected results.
- The Temkin-Pyzhev kinetic model was chosen as the subject for further investigation as the system responded as expected when subjected to varying temperatures and pressures.
- The power-optimal operating pressure was found to be at 235 bar.
- The optimal operating temperature for each reactor bed was 410°C for Bed 1, 420°C for Bed 2, and 415°C for Bed 3.

- The optimal length of each bed was found to be 1.132 m for Bed 1, 4.386 m for Bed 2, and 6.366 m for Bed 3, with a constant diameter of 3.0 m.
- The optimal void fraction for each bed was found to be 0.6 for Beds 1 & 2, and 0.85 for Bed 3.
- The system was able to produce 1166.7 kgmole/h, which corresponds to 19.9 tons/h of 98.25% ammonia (weight basis).
- All available heat was recovered by developing a HEN, which made the system functional without external heating required. The external cooling duty was lowered from 63.9 MW to 39.7MW with the proposed HEN.
- The energy efficiency for the system was calculated to 68.8% and the hydrogen efficiency was calculated to 93.4%.
- The power demand required for the process was calculated to 7.72 MW, which is sufficiently low to only use approximately 5% of the power output from the gas turbine.
- The purchase cost of the required equipment was estimated at 17.3 million US$. The ammonia synthesis reactor makes up about 82% of the total purchase cost for the process.
- The total capital investment was estimated to 87.6 million US$, of which 76.2 million US$ represents the total fixed capital, and 11.4 million US$ represents the working capital.

5.1 Further Work

After extensive simulation and work on this master thesis, a few key points stand out which could merit further work:

- Optimising the entire FPSO process, including the GTL process working in conjunction with the ammonia synthesis process would be a large undertaking, but would evaluate the system as a whole. This was not performed in this thesis due to the reasons outlined in Section 4.4.5. The process could be adjusted to produce different quantities of each product according to the market price.
- The current process design is heavily reliant on the kinetic model for ammonia synthesis. Even through the system response seemed to match conventional reactors, additional kinetic testing to ensure that the constants used, and that the models themselves are correct for the conditions which are simulated. This would give the system a more robust foundation.
- The feed streams of both hydrogen and nitrogen are streams coming directly from membranes. If the compositions of these streams were subject

to change, the process design would presumably also change. Thorough evaluation of these membranes should be performed to ensure that the stream compositions are correct.

- A thorough modelling of the ammonia synthesis reactor should be performed. In this simulation, 3 beds make up the reactor, but there is no guarantee that this is the optimal configuration.
- In certain cases, if the conversion rate in the reactor is high enough, a once-through configuration could be a viable option. This would however require an unconventional reactor, as conventional reactors cannot reach high conversion rates due to unfavourable equilibrium conditions. Such reactors do exist[11], but modelling one and implementing it in a simulation would require extensive reactor modelling as they do not conform to conventional reactor models.

Bibliography

[1] Alibaba. Ammonia catalyst cost. https://www.alibaba.com/product-detail/Ammonia-synthesis-catalyst-HTA110-1_505603975.html?spm=a2700.7724857.29.10.cIG35Y&s=p. [Online; accessed 19-June-2016].

[2] Alibaba. Methanation catalyst cost. https://www.alibaba.com/product-detail/Nickel-catalyst-with-al2O3-as-carrier_60033814583.html?spm=a2700.7724838.0.0.ZHFzr9&s=p. [Online; accessed 19-June-2016].

[3] I Chorkendorff and JW Niemantsverdriet. Concepts of Modern Catalysis and Kinetics. Weinheim: Wiley-VHC, 2007.

[4] Industrial Efficiency Technology Database. Ammonia synthesis. http://ietd.iipnetwork.org/content/ammonia-synthesis. [Online; accessed 19-June-2016].

[5] M Falkenberg and M Hillestad. Modeling, simulation and design of three different concepts for offshore methanol production, Submitted for publication.

[6] H Fogler. Elements of Chemical Reaction Engineering. Prentice Hall PTR, 2006.

[7] G Froment. Chemical Reactor Analysis and Design. Wiley, 1979.

[8] Magne Hillestand. Personal communications. norwegian university of science and technology (ntnu), 2016.

[9] J Jennings. Catalytic Ammonia Synthesis: Fundamentals and Practice. Wiley, 2013.

[10] Vincente Jiménez, Paula Sánchez, Paraskevi Panagiotopoulou, José Luís Valverde, and Amaya Romero. Methanation of co, co2 and selective methanation of co, in mixtures of co and co2, over ruthenium carbon nanofibers catalysts. Applied Catalysis A: General, 390:35–44, 2010.

[11] W. Kaboord, D. Becher, F. Begale, D. Fellers, and S. Kuznicki. Low pressure ammonia synthesis utilizing adsorptive enhancement, February 23 2006. US Patent App. 10/924,050.

[12] Kang Li. Ceramic Membranes for Separation and Reaction. Wiley, 2007.

[13] M Makkee, J.A Moulijn, and A.E VanDiepen. Chemical Process Technology. Wiley, 2013.

[14] G Mills and Fred W Steffgen. Catalytic methanation. Catalysis Reviews: Science and Engineering, 8:159–210, 1974.

[15] United States Geographical Survey Minerals. Annual ammonia production - 2015. `http://minerals.usgs.gov/minerals/pubs/commodity/nitrogen/mcs-2016-nitro.pdf`. [Online; accessed 19-June-2016].

[16] Mohammad Ostadi. Personal communications. norwegian university of science and technology (ntnu), 2016.

[17] Mohammad Ostadi, Kristin Dalane, Erling Rytter, and Magne Hillestad. Conceptual design of an autonomous once-through gas-to-liquid process - comparison netween fixed bed and microchannel reactors. Fuel Processing Technology, 139:186–195, November 2015.

[18] PotashCorp. Ammonia cost and natural gas price comparison. `http://www.potashcorp.com/overview/nutrients/nitrogen/overview/ammonia-cost-and-natural-gas-price-comparison`. [Online; accessed 19-June-2016].

[19] Ray Sinnott and Gavin Towler. Chemical Engineering Design. Amsterdam: Elsevier, 2009.

[20] Vaclav Smil. Detonator of the population explosion. Nature, 400(415), 1999.

[21] Vaclav Smil. Nitrogen cycle and world food production. World Agriculture, 2(9), 2011.

[22] NC State University. Composition of the atmosphere. `http://climate.ncsu.edu/edu/k12/.AtmComposition`. [Online; accessed 19-June-2016].

Appendix A

Appendix A

This appendix will include pictures of the HYSYS simulations for the two proposed process designs. The design utilising the membrane stream as a nitrogen source is given i Figure A.1, and the design utilising the tailgas is given in Figure A.2

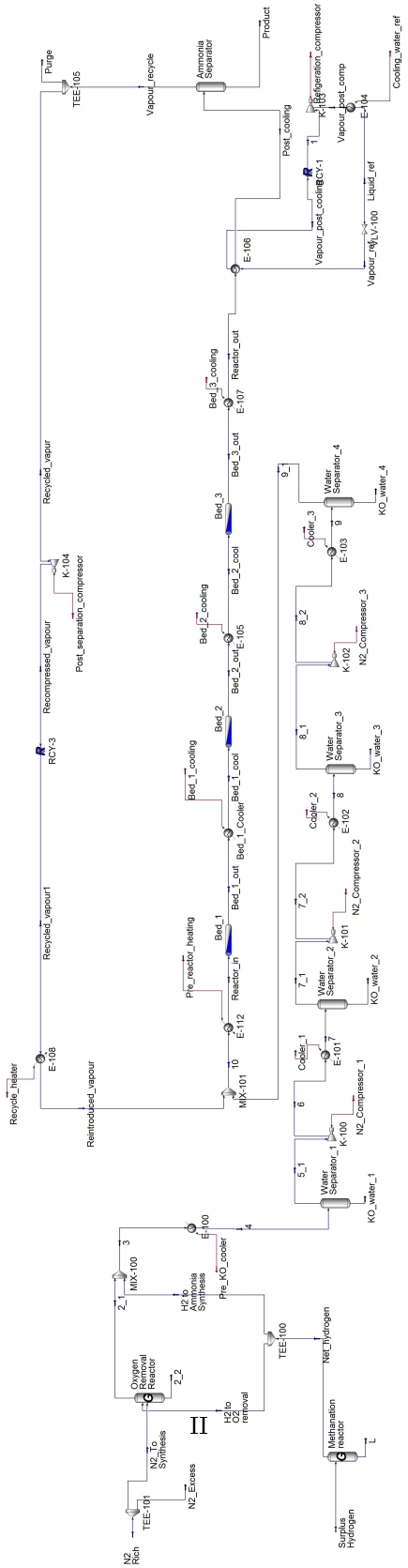

Figure A.1: HYSYS flow sheet for the system design utilising the membrane stream as a nitrogen source

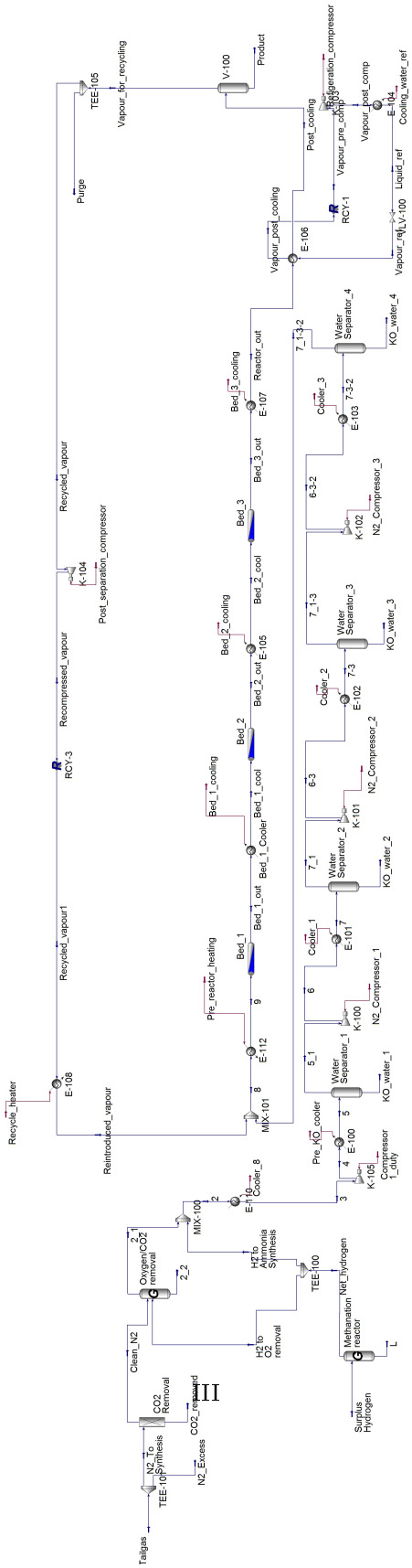

Figure A.2: HYSYS flow sheet for the system design utilising the tailgas

Appendix B

Appendix B

This appendix will give the stream properties for the process design featuring the nitrogen rich membrane stream. The process design featuring tailgas as the nitrogen source will not be given as it was not chosen for optimisation, as described in Chapter 4, and has the streams relevant for comparison given in Table 4.4.

B.1 Stream Properties

The process flow sheet for the optimised case which used the membrane stream as its nitrogen source is given in Figure B.1.

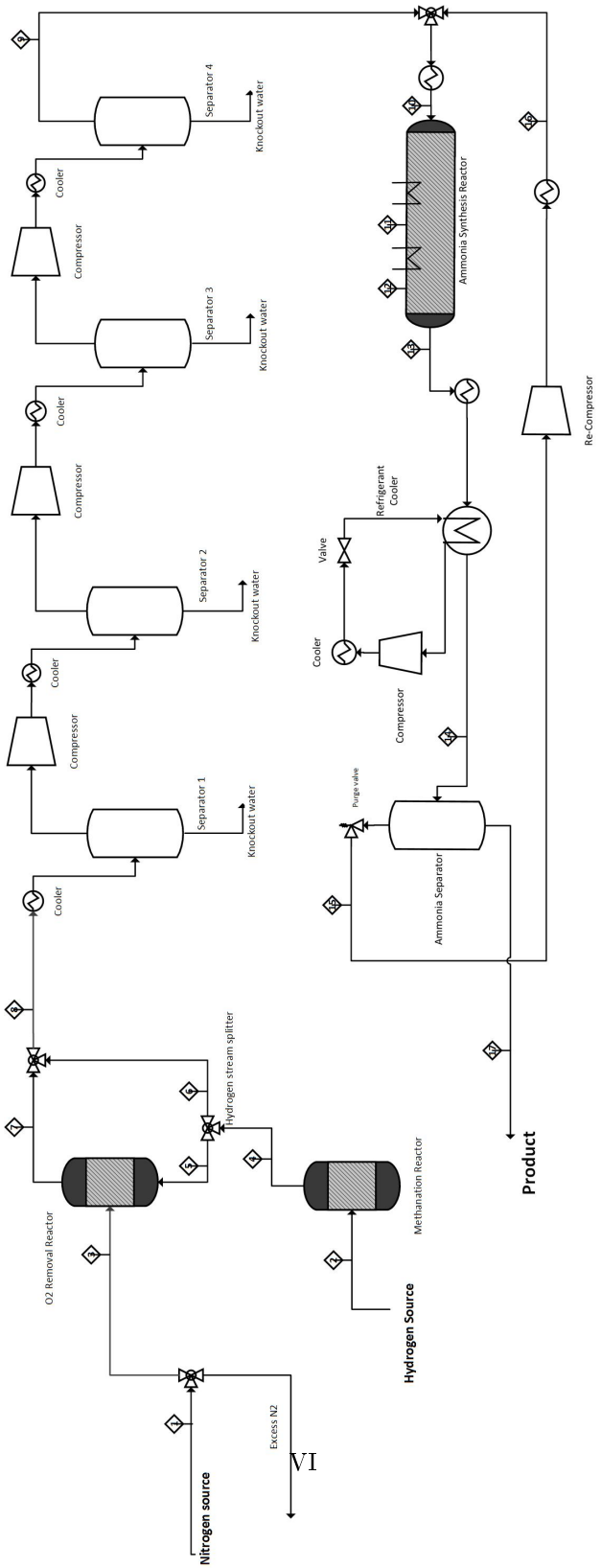

Figure B.1: The process flow sheet for the process design when using the N_2-rich membrane stream from the ASU as the nitrogen source

The stream properties for each stream as labelled in Figure B.1 is given in Tables B.1 and B.2.

Table B.1: The stream properties pertaining to streams 1-9 is labelled in Figure B.1.

Stream Number	1	2	3	4	5	6	7	8	9
Temperature [°C]	53.5	213.1	53.5	263.4	263.4	263.4	569.9	421.6	20.0
Pressure [kPa]	16 01	26 00	16 01	26 00	26 00	26 00	16 01	16 01	235 00
Molar Flow [kgmol/h]	7869	1889	613	1857	650	1207	1224	2432	2339
Mass Flow [kg/h]	221999	4474	17305	4474	1566	2908	18871	21779	20111
Mass Fractions [-]									
Carbon-Dioxide	0	0.1560	0	0	0	0	0	0	0
Nitrogen	0.9433	0	0.9433	0	0	0	0.8589	0.7442	0.8059
Oxygen	0.0567	0	0.0567	0	0	0	0	0	0
Hydrogen	0	0.8440	0	0.8154	0.8154	0.8154	0.0598	0.1607	0.1740
Ammonia	0	0	0	0	0	0	0.0075	0.0065	0.0070
Water	0	0	0	0.1277	0.1277	0.1277	0.0691	0.0770	0.0004
Methane	0	0	0	0.0569	0.0569	0.0569	0.005	0.0117	0.0126
Carbon-Monoxide	0	0	0	0	0	0	0	0	0

Table B.2: The stream properties pertaining to streams 10-17 is labelled in Figure B.1 .

Stream Number	10	11	12	13	14	15	16	17
Temperature [°C]	410.0	420	415.0	471.1	-16.0	-16.0	20.0	-16.0
Pressure [kPa]	235 00	230 00	225 00	220 00	220 00	220 00	235 00	220 00
Molar Flow [kgmol/h]	6748	6132	5805	5590	5590	4397	4409	1193
Mass Flow [kg/h]	61216	61216	61216	61216	61216	40993	41105	20223
Mass Fractions [-]								
Carbon-Dioxide	0	0	0	0	0	0.6481	0.6482	0
Nitrogen	0.7000	0.5591	0.4842	0.4350	0.4350	0	0	0.0031
Oxygen	0	0	0	0	0	0.1438	0.1438	0
Hydrogen	0.1537	0.1233	0.1071	0.0965	0.0965	0.0449	0.0449	0.0007
Ammonia	0.0324	0.2038	0.2948	0.3546	0.3546	0	0	0.9825
Water	0.0001	0.0001	0.0001	0.0001	0.0001	0	0	0.0004
Methane	0.1136	0.1136	0.1136	0.1136	0.1136	0.1631	0.1630	0.0132
Carbon-Monoxide	0.0001	0.0001	0.0001	0.0001	0.0001	0.0002	0.0002	0

Appendix C

Appendix C

In this appendix, the total mass and energy balance, and the energy efficiency for the process simulation is explained and calculated.

C.1 Mass Balance

The mass balance is important as it provides reassurance that mass is conserved in the system. The mass balance is given in Equation C.1

$$\dot{m}_{\text{in}} = \dot{m}_{out} \tag{C.1}$$

The values for each stream is taken directly from the HYSYS simulation, and is presented in table

Table C.1: The mass balance for the HYSYS simulation.

Inlet Streams	[kg/h]	Outlet Streams	[kg/h]
Surplus Hydrogen	4 474	Unused nitrogen source	204 694
Nitrogen Rich	221 999	Knockout water 1	1 611
		Knockout water 2	36.4
		Knockout water 3	14.7
		Knockout water 4	5.71
		Product	20 223
Sum	22 6473	Sum	22 6584

This amounts to a discrepancy of -111.3 kg/h. Using Equation C.2, this corresponds to -0.0005%, which is within acceptable limits. The discrepancy is probably due to the recycle function in Aspen HYSYS.

$$\text{d}\% = \frac{\dot{m}_{\text{in}} - \dot{m}_{out}}{\dot{m}_{\text{in}}} \tag{C.2}$$

C.2 Energy Balance

The energy balance for a system in steady state is formulated in Equation C.3

$$Q_{in} = Q_{out} \tag{C.3}$$

This can be further expanded according to the first law of thermodynamics, given in Equation C.4, to the equilibrium state of the sistem given in Equation C.5

$$Q_{in} = W_{out} - \dot{Q}_{in} \tag{C.4}$$

$$W_{out} - \dot{Q}_{in} = W_{in} - \dot{Q}_{out} \tag{C.5}$$

Equation C.5 is used in conjunction with the values given in the HYSYS simulation to calculate the energy balance for the system, given in Table C.2.

Table C.2: The Energy balance for the system with values from the HYSYS simulation.

Inlet Streams	Q [kJ/h]	Outlet streams	Q [kJ/h]
N2 Rich	5 763 254	Product	-83 004 236
Surplus Hydrogen	4 211 801	N2 Excess	5 314 008
		Knockout water 1	-2 558 3834
		Knockout water 2	-577 945
		Knockout water 3	-233 312
		Knockout water 4	-90 611
		Pre-KO cooler	33 051 414
Compressor 1	6 934 109	Cooler 1	7 048 476
Compressor 2	7 046 990	Cooler 2	7 115 114
Compressor 3	7 351 367	Cooler 3	7 308 060
Recompressor	912 394	Bed 1 cooling	31 034 119
Refrigeration Compressor	5 549 207	Bed 2 cooling	18 831 149
Heater 1	4 337 608	Bed 3 cooling	107 128 026
Heater 2	83 763 050	Cooling Water ref	18 442 729
Sum	125 869 780	Sum	125 783 155

The discrepancy amounts to 86 625 kJ/h, which equates to 0.0688%, which is regarded as acceptable. As with the mass balance, this discrepancy is probably due to the use of recycle functions in the simulation.

C.3 Energy Efficiency

The energy efficiency was calculated using heat flow for each component in the stream. These values are given as a part of the HYSYS fluid package (Peng-Robinson).

Table C.3 was used together with the stream information in HYSYS and the heat integration with the proposed HEN, described in Section 4.4 and Appendix E.1. Together they were used to calculate the energy efficiency in the process. The result is given in Table C.4.

Table C.3: The energy balance after heat integration.

Source	H [kJ/h]
Surplus Hydrogen	4 211 801
Nitrogen intake	449 246
Process-Process	215 539 698
Compressors	27 794 067
Sum	247 994 812

Out	
Ammonia product	-81 179 440
Unconverted H_2	-473 864
CO_2 converted to CH_4	-1 158 235
Knockout	-26 485 702
HP Steam	-72 323 363
MP Steam	-11 731 008
LP Steam	-10 451 371
Cooling water	-51 463 182
Sum	-255 266 165

When the heat integration with the proposed HEN, described in Section 4.4 and Appendix E.1, is included in the efficiency calculation, the energy efficiency of the proces can be calculated. The result i given in Table C.4.

Table C.4: An overview of where the energy from the inlet streams ends up.

Stream	Energy percentage [%]
Ammonia product	31.80%
Unconverted H_2	0.19%
CO_2 converted to CH_4	0.45%
Knockout	10.38%
HP Steam	28.33%
MP Steam	4.60%
LP Steam	4.09%
Cooling water	20.16%

In Chapter 4, the energy going towards cooling water, the energy in the knock-out water, the energy in unconverted hydrogen, and the energy in methane in the product stream are counted as "wasted" energy. From Table C.3, it becomes aparent that approximately 2.8% of the energy going in to the system is unaccounted for. This is probably due to the recycle function in the simulation, and possibly mistranslation of results from Aspen HYSYS to Aspen Energy Analyzer. The discrepancy is regarded as acceptable.

C.4 Hydrogen Efficiency

The hydrogen efficiency for the proces was calculated using the stream values from the HYSYS simulation and calculated with the data in Table C.4. Each component in Table C.5 has had its molar flow multiplied with it's hydrogen ratio compared to H_2, so ammonia was multiplied by $\frac{3}{2}$ and methane by 2.

Table C.5: An overview of where to hydrogen in the feedstock ends up.

Stream	H_2 content [kgmol/h]	Percentage of total H_2 content [%]
Hydrogen in		
Surplus Hydrogen	1873.1	
Hydrogen Out		
Knockout water 1	89.3	
Knockout water 2	2.02	
Knockout water 3	0.816	
Knockout water 4	0.317	
Sum Knockout water	92.5	4.94%
Ammonia product	1 750.0	93.43%
CO_2 converted to CH_4	33.3	1.78%
Unconverted H_2	6.81	0.36%
Water in product stream	0.494	0.03%

Appendix D

Appendix D

This appendix wil provide the data which was used to construct plots and figures in in the thesis. The data is presented in the order of which the figures or calculations appear in Chapter 4.
Tables D.1, D.2 and D.3 provide the basis for the values for the hydrogen split ratio calculation and Figures 4.3 4.4.

Table D.1: The simulated values which provides basis for the values for the hydrogen split ratio calculation and Figure 4.3.

Split Ratio [-]	O_2 Flow rate [kgmol/h]	CO_2 Flow rate [kgmol/h]	CO Flow rate [kgmol/h]	NH_3 Flow rate [kgmol/h]
0.00	30.668	0.000	0.000	0.000
0.01	21.303	0.159	0.000	0.000
0.02	11.937	0.317	0.000	0.000
0.03	2.571	0.476	0.000	0.000
0.04	0.000	0.533	0.101	0.012
0.05	0.000	0.555	0.237	0.046
0.06	0.000	0.577	0.367	0.096
0.07	0.000	0.592	0.488	0.162
0.08	0.000	0.589	0.584	0.242
0.09	0.000	0.560	0.637	0.336
0.10	0.000	0.501	0.635	0.441
0.12	0.000	0.338	0.503	0.684
0.14	0.000	0.194	0.324	0.977
0.16	0.000	0.103	0.188	1.332
0.18	0.000	0.055	0.106	1.756
0.20	0.000	0.030	0.061	2.251
0.22	0.000	0.017	0.036	2.819
0.24	0.000	0.010	0.022	3.460
0.26	0.000	0.006	0.014	4.175
0.28	0.000	0.004	0.009	4.964
0.30	0.000	0.003	0.006	5.825
0.32	0.000	0.002	0.004	6.757
0.34	0.000	0.001	0.003	7.760
0.36	0.000	0.001	0.002	8.831
0.38	0.000	0.001	0.001	9.967
0.40	0.000	0.000	0.001	11.168

Table D.2: The simulated values which provides basis for the values for the hydrogen split ratio calculation for the process design featuring the tailgas and Figure 4.4. Part 1/2.

Split Ratio [-]	CO_2 Flow rate [kgmol/h]	CO Flow rate [kgmol/h]	NH_3 Flow rate [kgmol/h]	O_2 Flow rate [kgmol/h]
0.01	6.18	0.00	0.00	6.96
0.02	6.13	0.21	0.00	0.00
0.03	5.61	0.89	0.00	0.00
0.04	5.25	1.41	0.01	0.00
0.05	4.98	1.83	0.01	0.00
0.06	4.79	2.18	0.02	0.00
0.07	4.64	2.48	0.03	0.00
0.08	4.53	2.75	0.03	0.00
0.09	4.44	2.98	0.05	0.00
0.10	4.36	3.17	0.06	0.00
0.12	4.22	3.48	0.09	0.00
0.14	4.02	3.64	0.12	0.00
0.16	3.73	3.64	0.16	0.00
0.18	3.36	3.48	0.20	0.00
0.20	2.94	3.21	0.24	0.00
0.22	2.51	2.87	0.28	0.00
0.24	2.10	2.49	0.32	0.00
0.26	1.71	2.10	0.37	0.00
0.28	1.37	1.73	0.42	0.00
0.30	1.08	1.39	0.48	0.00
0.32	0.83	1.10	0.54	0.00
0.34	0.63	0.84	0.61	0.00
0.36	0.47	0.64	0.69	0.00
0.38	0.35	0.48	0.77	0.00
0.40	0.26	0.36	0.86	0.00
0.42	0.19	0.27	0.96	0.00
0.44	0.14	0.20	1.07	0.00

Table D.3: The simulated values which provides basis for the values for the hydrogen split ratio calculation for the process design featuring the tailgas and Figure 4.4. Part 2/2.

Split Ratio [-]	CO_2 Flow rate [kgmol/h]	CO Flow rate [kgmol/h]	NH_3 Flow rate [kgmol/h]	O_2 Flow rate [kgmol/h]
0.46	0.11	0.15	1.18	0.00
0.48	0.08	0.11	1.31	0.00
0.50	0.06	0.08	1.44	0.00
0.52	0.05	0.06	1.58	0.00
0.54	0.04	0.05	1.73	0.00
0.56	0.03	0.04	1.88	0.00
0.58	0.02	0.03	2.04	0.00
0.60	0.02	0.02	2.21	0.00
0.62	0.01	0.02	2.39	0.00
0.64	0.01	0.02	2.58	0.00
0.66	0.01	0.01	2.77	0.00
0.68	0.01	0.01	2.97	0.00
0.70	0.01	0.01	3.18	0.00
0.72	0.00	0.01	3.39	0.00
0.74	0.00	0.01	3.61	0.00
0.76	0.00	0.00	3.84	0.00
0.78	0.00	0.00	4.08	0.00
0.80	0.00	0.00	4.32	0.00
0.82	0.00	0.00	4.57	0.00
0.84	0.00	0.00	4.82	0.00
0.85	0.00	0.00	4.95	0.00
0.87	0.00	0.00	5.22	0.00
0.90	0.00	0.00	5.63	0.00

Tables D.4 and D.5 contain the simulation data pertaining to once-through conversion at constant temperature for the two different kinetic models. The data is used to construct Figures 4.5 and 4.6.

Table D.4: The simulation data which provides the basis for conversion as a function of temperature for the Langmuir-Hinshelwood kinetic model in Figure 4.5.

Temperature [°C]	Conversion [%]	Temperature [°C]	Conversion [%]
20	9.02	285	1.21
30	10.63	295	0.97
40	12.29	305	0.75
50	13.68	315	0.57
60	14.28	325	0.41
70	14.03	335	0.27
80	13.37	345	0.15
90	12.58	355	0.04
100	11.76	365	-0.05
110	10.95	375	-0.13
120	10.15	385	-0.20
130	9.37	395	-0.26
140	8.61	405	-0.31
150	7.88	415	-0.36
160	7.17	425	-0.40
170	6.50	435	-0.43
180	5.85	445	-0.46
190	5.23	455	-0.49
200	4.66	465	-0.51
210	4.11	475	-0.53
220	3.60	485	-0.55
230	3.13	495	-0.56
240	2.70	505	-0.58
250	2.30	515	-0.59
260	1.95	525	-0.60
270	1.62	535	-0.61
280	1.34	545	-0.62

Table D.5: The simulation data which provides the basis for conversion as a function of temperature for the Temkin-Pyzhev kinetic model in Figure 4.6.

Temperature [°C]	Conversion [%]	Temperature [°C]	Conversion [%]
20	0.00		
30	0.00	295	0.17
40	0.00	305	0.23
50	0.00	315	0.31
60	0.00	325	0.42
70	0.00	335	0.56
80	0.00	345	0.74
90	0.00	355	0.96
100	0.00	365	1.25
110	0.00	375	1.61
120	0.00	385	2.06
130	0.00	395	2.61
140	0.00	405	3.28
150	0.00	415	4.10
160	0.00	425	5.09
170	0.00	435	6.26
180	0.00	445	7.62
190	0.00	455	9.08
200	0.00	465	10.39
210	0.01	475	11.24
220	0.01	485	11.49
230	0.02	495	11.30
240	0.02	505	10.89
250	0.03	515	10.39
260	0.05	525	9.86
270	0.07	535	9.32
280	0.10	545	8.80

Tables D.6 and D.7 contain the simulation data pertaining to conversion for two different temperatures as a function of pressure for the two different kinetic models. Tables D.6 and D.7 are used to construct Figures 4.7, 4.8, 4.9, and 4.10.

Table D.6: The simulation data used to construct figures 4.7 and 4.9 which is the conversion for two different temperatures as a function of pressure for the Langmuir-Hinshelwood kinetic model.

Pressure	L-H Kinetics Conversion at 60 °C[%]	L-H Kinetics Conversion 275 °C[%]
2000	14.41	1.80
2500	14.42	1.79
3000	14.43	1.78
3500	14.44	1.77
4000	14.45	1.76
4500	14.45	1.75
5000	14.46	1.73
5500	14.46	1.72
6000	14.47	1.71
6500	14.47	1.70
7000	14.47	1.69
7500	14.47	1.68
8000	14.47	1.67
8500	14.47	1.66
9000	14.47	1.65
9500	14.47	1.64
10000	14.46	1.63
11000	14.45	1.61
12000	14.44	1.59
13000	14.42	1.57
14000	14.39	1.55
15000	14.37	1.53
16000	14.34	1.51
17000	14.30	1.49
18000	14.26	1.47
19000	14.22	1.45
20000	14.18	1.43
21000	14.14	1.41
22000	14.10	1.40
23000	14.05	1.38
24000	14.01	1.36
25000	13.97	1.34

Table D.7: The simulation data used to construct figures 4.8 and 4.10which is the conversion for two different temperatures as a function of pressure for the Temkin-Pyzhev kinetic model.

Pressure [kPa]	T-P Kinetics Conversion at 480 °C[%]	T-P Kinetics Conversion at 275 °C[%]
2000	3.41	0.88
3000	5.01	1.50
4000	6.26	2.17
5000	7.30	2.88
6000	8.20	3.67
7000	8.99	4.55
8000	9.69	5.55
9000	10.33	6.73
10000	10.92	8.15
11000	11.46	9.96
12000	11.97	12.46
12500	12.20	14.15
13000	12.44	16.34
13500	12.66	19.21
14000	12.88	22.35
14500	13.09	24.45
15000	13.30	25.45
15500	13.50	25.92
16000	13.69	26.21
16500	13.88	26.43
17000	14.07	26.63
17500	14.25	26.82
18000	14.43	27.01
18500	14.60	27.18
19000	14.77	27.36
19500	14.94	27.53
20000	15.10	27.69
20500	15.26	27.85
21000	15.42	28.01
21500	15.57	28.17
22000	15.72	28.32
22500	15.87	28.47
23000	16.01	28.61
23500	16.15	28.75
24000	16.29	28.89
24500	16.43	29.03
25000	16.57	29.17

The simulation data in Table D.8 was obtained by observing the available hydrogen concentration when the amount of nitrogen introduced to the system

was steadily increased. The data was used to construct Figure 4.11.

Table D.8: The simulation data used to create Figure 4.11 which is hydrogen concentration before the inlet to the synthesis loop as a function of the split fraction for the nitrogen inlet stream.

Split [-]	Hydrogen Flow [kgmol/h]	Split [-]	Hydrogen Flow [kgmol/h]
0.01	1 791.6	0.37	1 734.3
0.02	1 773.5	0.38	1 733.4
0.03	1 755.4	0.39	1 732.5
0.04	1 750.8	0.4	1 731.6
0.05	1 751.2	0.41	1 730.7
0.06	1 751.6	0.42	1 729.7
0.07	1 752.0	0.43	1 728.8
0.08	1 752.1	0.44	1 727.8
0.09	1 752.0	0.45	1 726.7
0.10	1 751.6	0.46	1 725.7
0.11	1 751.0	0.47	1 724.6
0.12	1 750.2	0.48	1 723.6
0.13	1 749.4	0.49	1 722.5
0.14	1 748.7	0.5	1 721.3
0.15	1 748.0	0.51	1 720.2
0.16	1 747.4	0.52	1 719.1
0.17	1 746.8	0.53	1 717.9
0.18	1 746.3	0.54	1 716.7
0.19	1 745.8	0.55	1 715.5
0.2	1 745.3	0.56	1 714.3
0.21	1 744.8	0.57	1 713.1
0.22	1 744.3	0.58	1 711.8
0.23	1 743.8	0.59	1 710.5
0.24	1 743.3	0.6	1 709.3
0.25	1 742.8	0.61	1 708.0
0.26	1 742.2	0.62	1 706.7
0.27	1 741.6	0.63	1 705.4
0.28	1 741.0	0.64	1 704.1
0.29	1 740.3	0.65	1 702.7
0.3	1 739.7	0.66	1 701.4
0.31	1 739.0	0.67	1 700.0
0.32	1 738.3	0.68	1 698.7
0.33	1 737.5	0.69	1 697.3
0.34	1 736.8	0.7	1 695.9
0.35	1 736.0	0.71	1 694.5
0.36	1 735.1	0.72	1 693.1

In Tables D.10 and D.9, the power consumption of all compressors was simulated

as a function of the operating pressure in the synthesis loop, including the pre-loop compressor, the refrigeration compressor, and the compressor in the synthesis loop which accounts for pressure drop in the reactor. The simulation data was used to construct Figures 4.12 and 4.13. The power consumption is given in individually in Table 4.13, and combined in Table D.10. The reson for this was to observe the power consumption as a function of operating pressure for each compressor, as the result given in Figure 4.12 indicated each compressure had a unique power consumption function which would account for the minima point. This is confirmed both from the graphical data in Figures 4.12 and 4.13, as well as from the simulation data in Tables D.9 and D.10.

Table D.9: The simulation data used to plot Figure 4.13.

Pressure [kPa]	Re-compression Compressor [kW]	Refrigeration Compressor [kW]	Pre-Loop Compressors[kPa]
10000	2 857	5 939	3 810
12500	1 492	4 876	4 335
15000	967.3	3 777	4 778
17500	695	3 016	5 162
20000	528.5	2 522	5 503
21000	484.5	2 401	5 630
22500	429.5	2247	5 810
23000	413.5	2 202	5 869
23500	398.6	2 159	5 925
24000	384.6	2 118	5 982
24500	371.4	2 080	6 036
25000	359	2 043	6 092
27500	306.6	1 886	6 350
30000	266.5	1 761	6 591
32500	230.5	1 622	6 815
35000	205.8	1 541	7 028

Table D.10: The power consumption for all compressors as a function of operating pressure used to plot Figure 4.12.

Pressure [bar]	Total Power Consumption [MW]
100	12.606
125	10.703
150	9.5223
175	8.873
200	8.5535
210	8.5155
225	8.4865
230	8.4845
235	8.4826
240	8.4846
245	8.4874
250	8.494
275	8.5426
300	8.6185
325	8.6675
350	8.7748

The simulation data in Table D.11 is the conversion rate of each individual reaction bed as a function of inlet temperature. The data is given individually in Figures 4.14, 4.15 and 4.16 to display correct physical behaviour.

Table D.11: The conversion rate of each rection bed as a function of temperature.

	Conversion [%]		
Temperature [°C]	Bed 1	Bed 2	Bed 3
400	19.00	8.95	7.44
405	19.55	10.16	8.02
410	19.62	11.28	8.43
415	19.46	11.96	8.61
420	19.20	12.20	8.58
425	18.89	12.18	8.46
430	18.56	11.98	8.14
435	18.22	11.66	7.73
440	17.89	11.27	7.26
445	17.55	10.84	6.76
450	17.21	10.39	6.23
455	16.87	9.93	5.69
460	16.54	9.46	5.15
465	16.21	8.99	4.59
470	15.88	8.51	4.03
475	15.56	8.05	3.48
480	15.24	7.57	2.92
485	14.92	7.10	2.39
490	14.60	6.64	1.83
495	14.29	6.17	1.29
500	13.97	5.71	0.77

The sizing of each reactor bed was done by udjusting the dimensions of the reactor as well as the void fraction given in Table 4.6 in Section 4.3. Teh diameter is kept constant is 3.00 m for all three beds. The temperature curve and the reaction rate curve for each bed is given in Figures D.1 and D.2 for Bed 1, Figures D.3 and D.4 for Bed 2, and Figures D.5 and D.6 for Bed 3.

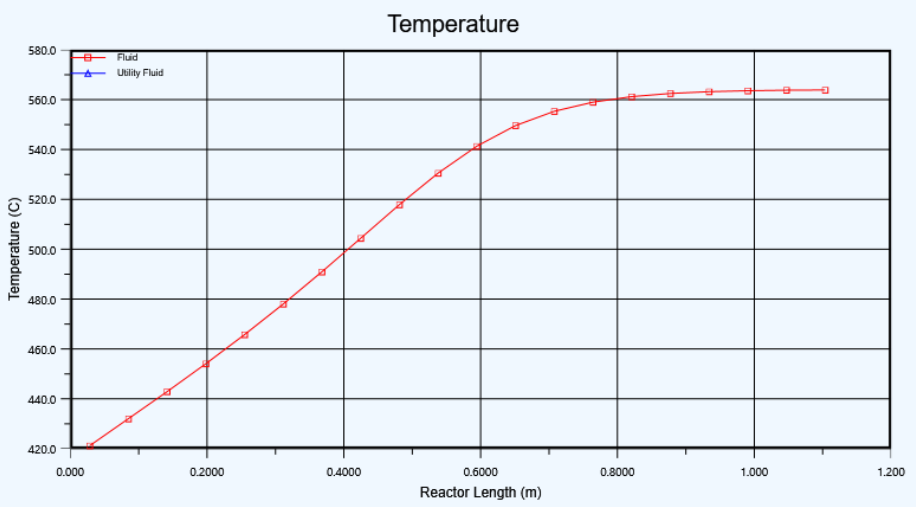

Figure D.1: The temperature in the reactor as a function of distance from the inlet for Bed 1.

Figure D.2: The formation rate of ammonia as a function of distance from the reactor inlet for Bed 1.

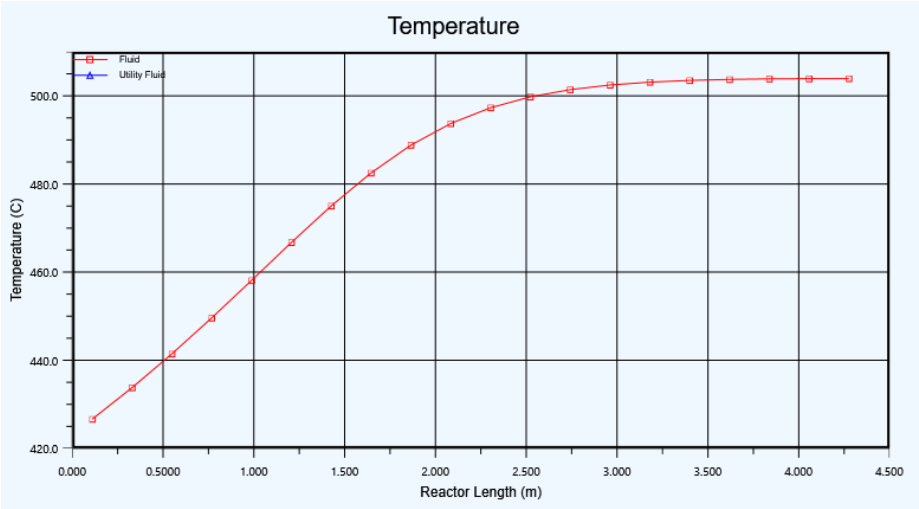

Figure D.3: The temperature in the reactor as a function of distance from the inlet for Bed 2.

Figure D.4: The formation rate of ammonia as a function of distance from the reactor inlet for Bed 2.

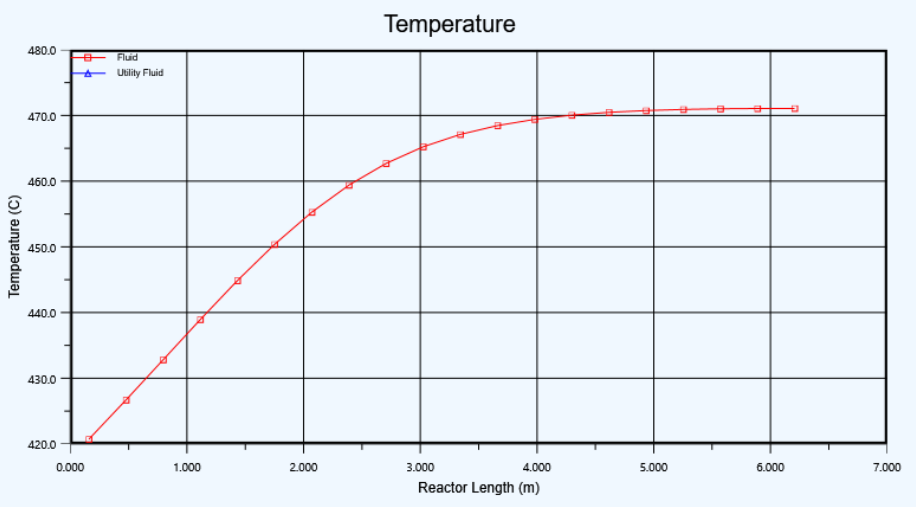

Figure D.5: The temperature in the reactor as a function of distance from the inlet for Bed 3.

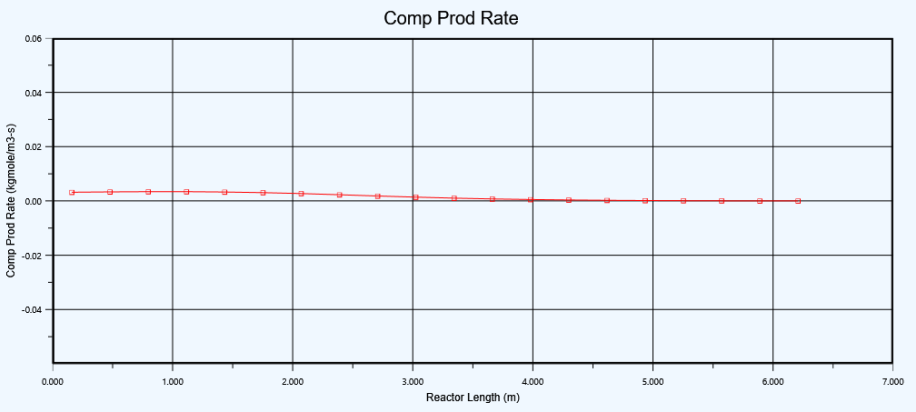

Figure D.6: The formation rate of ammonia as a function of distance from the reactor inlet for Bed 3.

Appendix E

Appendix E

This appendix will provide the basis for the heat integration done for the system.

E.1 Heat Integration Basis

In Table E.1, the specifications for the Base Case HEN proposed by Aspen Energy Analyzer is given.

Table E.1: Heat exchanger specifications for the Base Case scenario.

Unit name	Utility	Area [m^2]	Number of shells [-]	Load [kJ/h]
Bed_1_Cooler@Main	HP Steam	58.7	1	31 034 098
E-100@Main	Refrigerant	125.9	2	33 051 413
E-103@Main	Refrigerant	47.7	1	7 308 059
E-105@Main	HP Steam	41.5	1	18 831 075
E-109@Main	Refrigerant	79.9	1	12 894 110
E-101@Main	Refrigerant	87.4	1	7 048 476
E-102@Main	Refrigerant	62.7	1	7 115 113
E-107@Main	Refrigerant	167.7	1	98 257 350
E-108@Main	LP Steam	11.9	1	4 250 453
E-112@Main	Fired Heat	617.1	2	83 763 050

The details for each heat exchanger in the Base Case HEN is given in Table E.2. Table E.3 provides the specification for the top 10 HENs proposed by Aspen Energy Analyzer.

Table E.2: The specification for the Base Case HEN.

Unit name	Load [kJ/h]	Hot Stream Name	T_{in}	T_{out}	Cold Stream Name	T_{in}	T_{out}
Bed_1_Cooler @Main	31 034 098	Bed_1_out_To_Bed_1_cool	564	420	HP Steam Generation	249	250
E-100@Main	33 051 413	3_To_4	422	20.0	Refrigerant 1	-25.0	-23.9
E-103@Main	7 308 059	8_2_To_9	121	20.0	Refrigerant 1	-25.0	-23.9
E-105@Main	18 831 075	Bed_2_out_To_Bed_2_cool	504	415	HP Steam Generation	249	250
E-109@Main	12 894 110	Bed_3_out_To_Post_cooling	72.3	20.0	Refrigerant 1	-25.0	-23.9
E-101@Main	7 048 476	6_To_7	121	20.0	Refrigerant 1	-25.0	-23.9
E-102@Main	7 115 113	7_2_To_8	121	20.0	Refrigerant 1	-25.0	-23.9
E-107@Main	98 257 350	Bed_3_out_To_Post_cooling	471	72.3	Refrigerant 1	-25.0	-24.0
E-108@Main	4 250 453	LP Steam	125	124	Recompressed_vapour_To_Reintroduced_vapour	-9.59	20.0
E-112@Main	83 763 050	Fired Heat (1000)	1000	400	10_To_Reactor_in	19.8	410

Table E.3: The top 10 HENs as proposed by Aspen Energy Analyzer.

Design number	Area [m^2]	Number of heat exchangers [-]	Number of shells [-]	Cooling required [kJ/h]
A_Design80	2 877	16	34	142 843 879
A_Design69	2 901	18	33	165 246 492
A_Design54	2 766	18	34	142 850 987
A_Design58	2 794	16	31	172 366 242
A_Design26	2 720	16	34	142 852 488
A_Design83	2 702	18	32	147 665 320
A_Design59	2 653	18	34	147 678 136
A_Design43	2 684	18	32	147 663 344
A_Design7	2 710	16	33	142 850 987
A_Design88	2 619	18	32	165 246 492

Appendix F

Appendix F

This appendix will deal with the calculations performed when sizing the equipment used in this ammonia synthesis process. All vessels are calculated as pressure vessels made from 304 Stainless Steel with a density of 8 $000 kg/m^3$.

F.0.1 Calculating the Mass of a Pressure Vessel

To calculate the mass for each pressure vessel, the shell thickness (t_w) will have to be calculated, as shown in Equation F.1

$$t_w = \frac{PD_v}{2SE - 1.2P} \tag{F.1}$$

Where D is the vessel diameter, P is the design pressure, in all cases set to equal 15% of the operating pressure, S is the allowable stress calculated by using the operating temperature and F.1 as described in Sinnot & Towler[19] and E is the welding efficiency, in all cases set to equal 1.

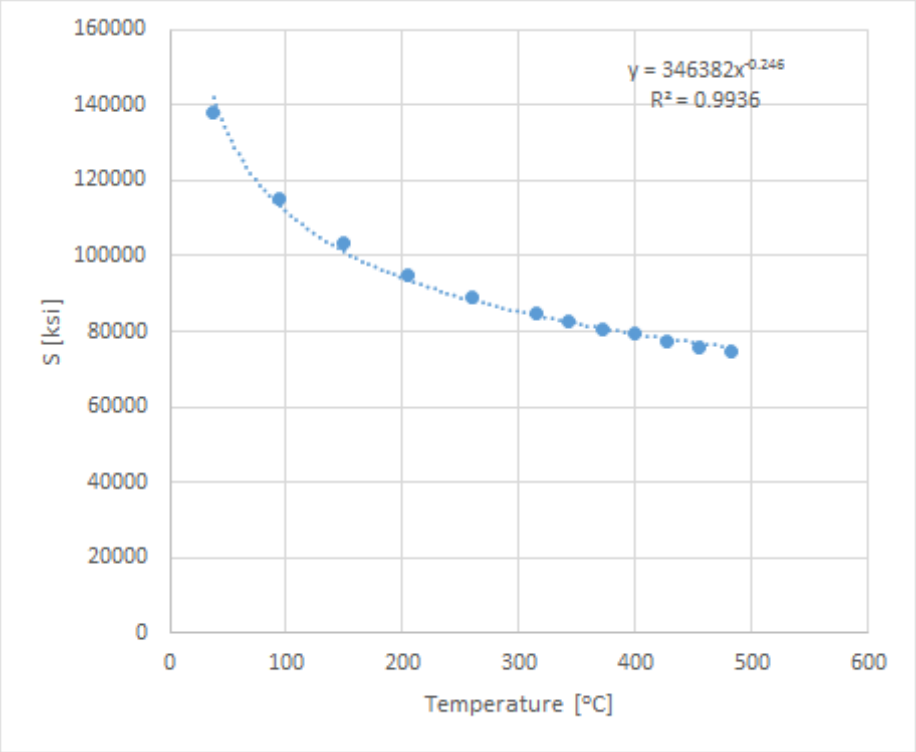

Figure F.1: The allowable stress as a function of operating temperature

The surface area of the pressure vessel is calculated as a cylinder, as shown in Equation F.2

$$A_s = \pi D_v H \tag{F.2}$$

Where H is the vessel height and A_s is the vessel surface area and D_v is the vessel diameter.

The head of the vessel is assumed to be an eliptical head. The required wall thickness is calculated in Equation F.3

$$t_{w_{head}} = \frac{PD_v}{2SE - 0.2P} \tag{F.3}$$

The eliptical head surface area, A_h is given in Equation F.4

$$A_h = 1.09D_v^2 \tag{F.4}$$

The mass of the pressure vessel is then calculated as shown in Equation F.5

$$m = \rho_m t_w (A_s + 2A_h) \tag{F.5}$$

F.0.2 Calculating the Volume Required by a Vessel

To calculate the outer volume required by a pressure vessel, the outer height of the eliptical head (H_h) has to be calculated, and is shown in Equation F.6. It is assumed that the straight flange (S.F) is equal to that of $3t_w$

$$H_h = 0.25D_v + 3S.F + t_w = 0.25D_v + 4t_w \tag{F.6}$$

Simple geometry shows that the outer diameter and height (D_{outer} and H_{outer}) is found as in Equation F.7 and Equation F.8 respectively

$$D_{outer} = D_v + 2t_w \tag{F.7}$$

$$H_{outer} = H + 2H_h \tag{F.8}$$

The volume of the shell (V_{shell}) can be calculated as shown in Equation F.9

$$V_{shell} = \frac{\pi D_{outer}^2 H_{outer}}{4} \tag{F.9}$$

and the volume of the eliptical head (V_{head}) as in Equation F.10

$$V_{head} = \frac{\pi D_{outer}^3}{24} + \frac{\pi D_{outer}^2 3t_w}{4} \tag{F.10}$$

making the total volume required by the vessel (V_{tot}) to be as in Equation F.11

$$V_{tot} = V_{shell} + V_{head} \tag{F.11}$$

F.0.3 Two Phase Separators

The sizing of the two phase separators are done is described for vertical separators in Sinnott and Towler [19].

The settling velocity, u_s, is a function of the density for the relevant liquid and gas (ρ_l and ρ_g respectively), ans is calculated as shown in Equation F.12

$$u_s = 0.07\sqrt{\left(\frac{\rho_l - \rho_g}{\rho_g}\right)} \tag{F.12}$$

The minimum vessel diameter (D_v) for droplett settling to occur is calculated by using the volumetric gas flow rate, $\dot{V_g}$, and Equation F.13

$$D_v = \sqrt{\frac{4\dot{V_g}}{\pi u_s}} \tag{F.13}$$

Assuming a residence time in the separator of t =10 minutes, the height of the separator is calculated by equation F.14

$$D_v = \frac{\dot{V}_g t}{0.25\pi D_v^2} \tag{F.14}$$

The height of the separator, H, can now be calculated as shown in Equation F.15

$$H = h_v + \frac{D_v}{2} + D_v + 0.4 \tag{F.15}$$

F.0.4 Methanation and Ammonia Reactor Sizing

The reactor volume for the methanation reactor is calculated by using the gas hourly space velocity found in literature,[14] to find the catalyst volume (V_c) needed for the reactor. The GHSV used for the reactor is 10 000 h^{-1}

The catalyst volume is found by using Equation F.16

$$V_c = \frac{\dot{V}}{GHSV} \tag{F.16}$$

Where $\dot{V}$ is the volumetric gas feed flow given in HYSYS.

It is assumed that the catalyst accounts for 50% of the total volume (V_{tot}) in the methanation reactor. The catalyst volume is specified in HYSYS for the ammonia synthesis reactor. For simplicity, the ratio between the length and the diameter is set to 1.5 for the methanation reactor. From this, and Equation F.17 the diameter for each reactor can now be calculated

$$D = \left(\frac{8V_{tot}}{3\pi}\right)^{1/3} \tag{F.17}$$

Appendix G

Appendix G

This section will deal with the calculations done when performing a cost estimation for the equipment used in the best case scenario of the ammonia synthesis process as stated in the conclusion i Chapter 5.

G.0.1 Compressor Cost Estimation

For calculating the cost of the compressor, matche.com cost estimator was used. The equipment selected was a centrifugal compressor with a 650 psi setting operating at the specified duty in each case, as shown in Table G.1

Table G.1: The calculated cost of each compressor as a function of duty using matche.com estimator.

Name	Duty [kW]
K-100	1,926
K-101	1,957
K-102	2,042
Refrigeration Compressor	1,541
K-104	253

G.0.2 Heat Exchanger and Pressure Vessel Cost Estimation

The purchase equipment cost was calculated as shown in Equation G.1 as described in Sinnott and Towler[19].

$$C_e = a + bS^n \tag{G.1}$$

The values for a, b, S and n varies with each different type of equipment according to the information given in Table G.2.

Table G.2: The values used with Equation G.1 to calculate the purchase cost for each type of equipment.

Equipment	S	a	b	n
Heat Exchangers	Heat Transfer Area [m^2]	24000	46	1,2
Vertical Pressure Vessel	Shell mass [kg]	15000	68	0,85

The two-phase separators used for water removal before the synthesis loop, the ammonia separator and the Oxygen Removal Reactor are all considered vertical pressure vessels in this respect.

G.0.3 Catalyst Cost Estimation

The cost for each catalyst was calculated based on the dimensions for each reactor calculated in Appendix F.0.4. The basis for the calculations are given in Table G.3.

Table G.3: The catalyst cost estimation for the two catalytic reactions in the ammonia synthesis process.

Name	Methanation Reaction	Ammonia Synthesis
Catalyst Type	Nickel on Alumina	Iron(III)Oxide on Alumina
Catalyst Volume [%]	50%	32%
Reactor Volume [m^3]	0.593	84
Catalyst Volume [m^3]	0.296	26.6
Catalyst Density [kg/m^3]	807.5	2 800
Catalyst Weight [kg]	239.3	74 480
Catalyst Cost [$/kg] [2][1]	21.00	5.00

G.0.4 PPC and Fixed Capital Estimation

All estimated costs in Chapter 4 included in the PCE has had its cost adjusted with the CEPCI index given in Table G.4

Table G.4: The CEPCI Index, used to adjust prices due to inflation effects.

Year	CEPCI
1985	325
2005	468,2
2006	499,6
2007	525,4
2008	575,4
2009	525,4
2010	550,8
2011	585,7
2012	584,6
2013	567,3
2014	575,5
2015	550,4

The PPC was calculated using the total equipment cost, PCE, the factors given in Table G.5, and Equation G.2. Other factors normally associated with calculating PPC such as structures and civil are not included in the calculations as they are not relevant to installing equipment in a FPSO.

Table G.5: Installed equipment cost factors.

Category	Symbol	Factor
Equipment Erection	f_1	0,40
Piping	f_2	0,70
Instrumentation and Control	f_3	0,20
Electrical	f_4	0,20
Material factor, 304 SS	f_5	0,15
Utilities	f_6	0,50
Lagging and paint	f_7	0,10
Design and Engineering	f_8	0,30

$$PPC = PCE(1 + f_1 + f_2 + f_3 + f_4 + f_5 + f_6) \tag{G.2}$$

The total fixed capital is then calculated by Equation G.3

$$TotalFixedCapital = PPC(1 + f_7 + f_8) \tag{G.3}$$

G.0.5 Calculation of Working Capital, ISBL, OSBL and the Total Capital Investment

The equations for calculating the working capital, ISBL, OSBL and the total capital investment are given in Equations G.4 to G.7.[19]

$$WorkingCapital = TotalFixedCapital \cdot 15\% \tag{G.4}$$

$$ISBL = \frac{TotalFixedCapital}{1.82} \tag{G.5}$$

$$OSBL = TotalFixedCapital - ISBL \tag{G.6}$$

$$TotalCapitalInvestment = TotalFixedCapital + WorkingCapital \tag{G.7}$$